THE PREDICTION OF THE INTERACTION BETWEEN SHIPBOARD ANTENNAS AND THEIR ENVIRONMENT

Louis Botha

A dissertation submitted to the Faculty of Engineering, University of the Witwatersrand, Johannesburg, in fulfillment of the requirements for the degree of Master of Science in Engineering.

Johannesburg, 1991.

DECLARATION

I declare that this dissertation is my own, unaided work. It is being submitted for the Degree of Master of Science in Engineering at the University of the Witwatersrand, Johannesburg. It has not been submitted before for any degree or examination in any other University.

30 th day of April 1991

ABSTRACT

This dissertation discusses the interaction between shipboard antennas and their environment.

The emphasis is on the use of the Method of Moments to calculate the currents on the structure of the ship. These currents are induced by the antennas mounted on the structure of the ship.

The parameters (such as grid spacing and wire radius) to use in creating a wire grid model of the ship is investigated and recommended values given.

A sample ship is analyzed and the results obtained compared with measurements done in an anechoic chamber.

ACKNOWLEDGEMENTS

The author would like to acknowledge the help and suggestions of his supervisor, Prof Hanrahhan. The author would also like to acknowledge the help of Dr B. A. Austin under whose supervision this dissertation was started.

The author is indebted to his employers, the CSIR, for support of his research and permission to publish this work.

Dedicated to Celesté.

Table of Contents

Table of Figures

Table of Tables

LIST OF SYMBOLS

E	Electric field
f	frequency
H	Magnetic field
I	Current
J	Current density
k	Propagation constant
r	distance from origin
t	time
V	Voltage
x	first coordinate in rectangular coordinate system
y	second coordinate in rectangular coordinate system
z	third coordinate in rectangular coordinate system
λ	wavelength
ω	wavenumber - defined as $2\pi f$
θ	angle between z axis and vector in spherical coordinate system

ϕ	angle between x axis and projected vector in x-y plane in spherical coordinate system
$^{\circ}$	degree
ρ	vector in x-y plane in cylindrical coordinate system
Λ	mathematical del operator

NOMENCLATURE

dB	decibel
DF	Direction Finding
EFIE	Electrical Field Integral Equation
EMP	Electromagnetic Pulse
ESP	Computer program with surface formulation
GHz	Gigahertz
GTD	Geometrical Theory of Diffraction
HF	High Frequency (2 - 30 MHz)
MFIE	Magnetic Field Integral Equation
MHz	Megahertz
MM	Method of Moment
NEC2	Computer program developed at Lawrence Livermore National Laboratories
RADHAZ	Radiation Hazard
RCS	Radar Cross Section
RF	Radio Frequency

THWIRE	Computer program developed at Ohio State University
UHF	Ultra High Frequency (300 - 3000 MHz)
VHF	Very High Frequency (30 - 300 MHz)
VSWR	Voltage Standing Wave Ratio

1 INTRODUCTION

1.1 The need for prediction

The various elements of a ship's superstructure such as the masts, funnels and different decks constitute a complex scattering and reradiating environment for any antenna. Any antenna located within such an environment will possess radiating characteristics considerably different from the same characteristics under free space conditions.

Degradation from the ideal is most apparent with wide beamwidth antennas, especially omnidirectional antennas such as those required for certain forms of communications and Direction Finding (DF) systems. Departure from the ideal free space behavior leads to errors in DF systems and to less than optimum performance for communication systems.

Unfortunately, these antennas cannot be sited so that their radiation patterns are unaffected by any neighboring superstructure or any other antenna system. This is because no antenna can exist in isolation on a ship's crowded decks and masts. Figure 1.1 shows a typical view of antennas on a ship. At best one must try a number of different antenna locations to find the location where the unwanted effects of the superstructure on the antenna are minimized.

In this thesis I will use the term radiation pattern even for a receiving antenna because of reciprocity. The reciprocity theorem ([1] p 40) states that the radiation and receiving patterns of an antenna are exactly the same.

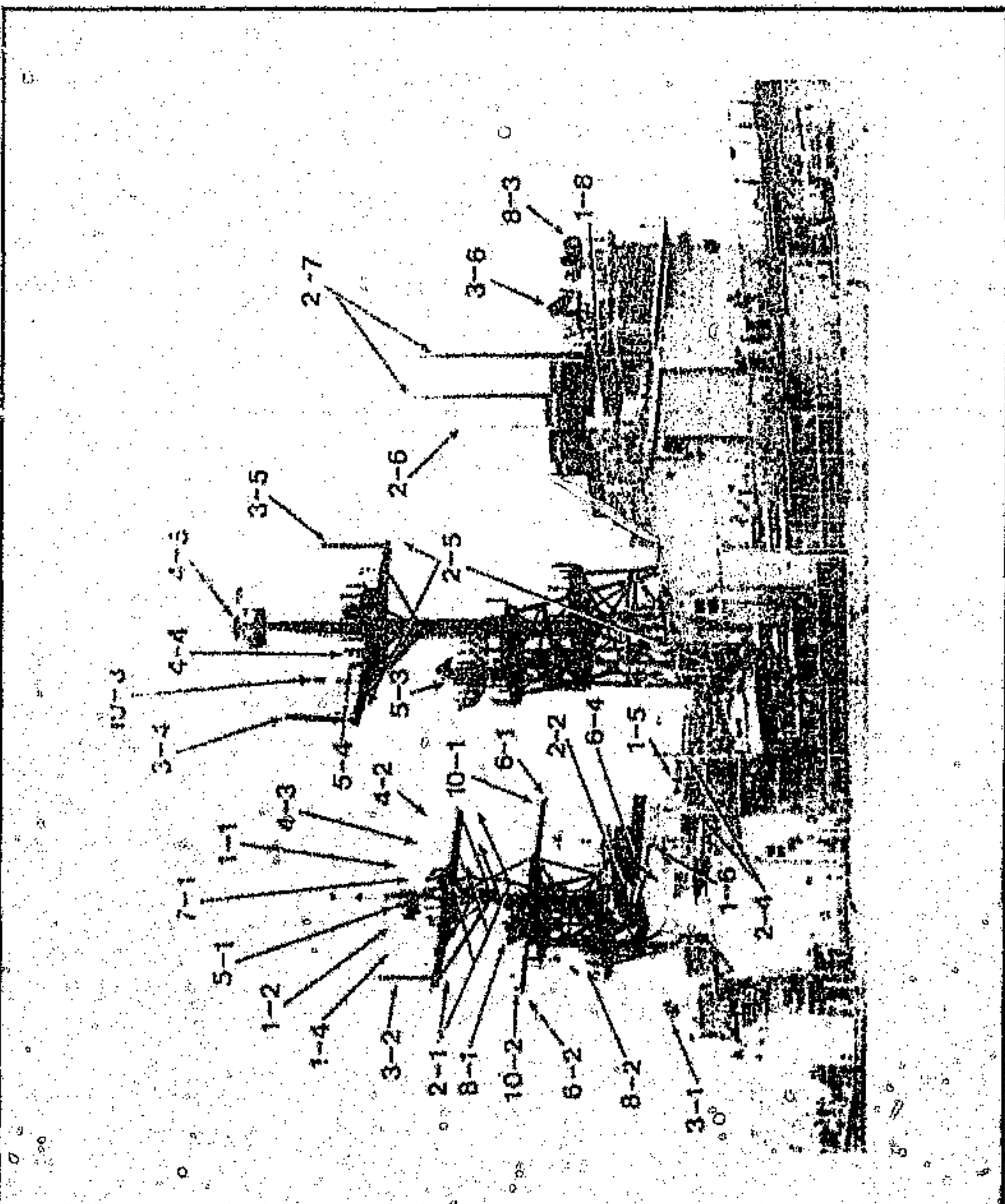

Figure 1.1 A typical view of antennas on a ship. (From [24])

There are several different antenna related problems that appear on a complex platform. The first problem is the degradation of the radiation pattern of the antennas. The degradation of the radiation pattern may take the form of a blockage in the pattern where there may be loss of signal (and thus communication) in a specific direction. It may also be in the form of multipath where a signal may be received by more than one path (some direct rays and others reflected or diffracted rays). The different rays will then add in and out of phase and so created a distorted pattern.

If structures in the near field of the antenna are excited such that currents comparable to the size of the currents on the antennas begin to flow, the actual currents on the antenna will be changed. This will not only cause problems in the radiation pattern of the antenna, but also in the impedance (and thus in the VSWR) of the antenna. This means that less power is being transmitted, and that some equipment will not work properly or may even be damaged by the reflected power.

Because of the close proximity of the antennas on the platform, the level of reception of an undesired signal by an antenna is increased. An example is a communication transmission being received on an navigation antenna. The level of this undesired signal must be controlled as far as possible for acceptable system performance to be obtained. This is usually done by mounting antennas connected to high power transmitters as far as possible away from antennas connected to sensitive receivers.

A problem that is getting more attention lately is the problem of radiation hazards (RADHAZ). This is where the level of electric energy is so large that it possess a hazard to personnel (for example a worker in front of a high power radar antenna) or to fuel and explosives. For effective control of RADHAZ the energy levels at different places on the ship must be known. If areas with high RF power levels are identified, control measures such as the establishment of restricted areas around transmit antennas can be taken.

The single most important reason why a method to predict the performance of an antenna in the presence of the ship is needed, is because of the high cost of moving antenna installations on ships. A further problem is the measurement of the radiated field from an antenna installed on a ship.

By using methods to predict the performance of the antennas in the presence of the ship, it is possible to try a fair number of different antenna locations to find an optimum location. Such an option is much cheaper than to install antennas using trail and error techniques.

Prediction methods can also be used as diagnostic tools to try and solve problems in existing installations by giving the analyst more insight into the physics of radiation characteristics.

1.2 Preview of work

The next paragraph (1.3) gives a summary of earlier work in prediction. Paragraph 1.4 gives a summary of the various prediction methods available such as model measurement, the Method of Moments, Geometrical Theory of Diffraction and hybrid methods.

The Method of Moments is the subject of chapter 2. After an introduction, the Moment Method is described. The three computer programs used in this study are then described. A study is described to verify the Method of Moments using dipoles. The parameters necessary to model a solid surface with a wire grid are determined. The chapter is ended with a short discussion of the results.

Chapter 3 discusses the results obtained during the modelling of a ship. Three models of increasing complexity are described and the results shown. At the end of the chapter a discussion of the results is given.

Chapter 4 shows the conclusions drawn from the results obtained. After a summary of the results, further possible extensions are discussed.

The references used are shown in chapter 5.

Appendix A shows the details of some integral equations.

Appendix B shows the details of the measurements made on the ship model.

Appendix C shows the result of the dipole study in tabular form.

Appendix D and E show respectively the derivation of the necessary wire radius to use for square and triangular meshes.

1.3 Earlier work in prediction

Moore and Pizer[2] give a very good introduction into the Method of Moments. The most important integral equations are described. Some computer codes that the authors have used are described. Several practical applications of the Method of Moments are also discussed in this book. One of the important aspects discussed is the use of wire grid modelling for the modelling of solid surfaces. Although the work in their book is based on scattering problems, it gave a very good starting point for the antenna on ship problem.

Butler and Wilton [3] show several numerical techniques to solve Pocklington's and Hallen's equations for thin-wire scatterers. The basis functions considered include the piecewise sinusoidal, piecewise linear and trigonometric functions. Various types of testing schemes such as collocation and Gälerkin are used. The authors come to the conclusion that to obtain acceptable convergence rates, discontinuities in the current approximation and its derivatives must be suppressed. Another useful technique is to circumvent the effect of such discontinuities by making the equation insensitive to them. This may be done by using averaging techniques such as using a Galerkin technique.

Pearson and Butler [4] discuss the inadequacies of the collocation solutions to Pocklington-type models of thin-wire structures. The basis functions under discussion are the piecewise sinusoidal functions. It is shown that with point matching this type of basis function has little utility.

Richmond [5] introduces the principle of using a wire grid to model a continuous surface. He uses an uniform current density on each segment with point matching at the center of the segments. Scattering from the surfaces is modelled. He was able to solve problems with a maximum of 100 unknowns, that is, up to one square wavelength in size. A circular plate of radius 0,15 λ was modelled with 3 polygonal rings (20 sides each) at radii of 0,05, 0,10 and 0,15 λ. The center of the plate was left open. The wire radius was taken as 0.005 λ. A square plate, with size that changed from 0,3 to 1,1 λ, was modelled with 8 wires in each direction. The wire diameter was taken to be $\frac{1}{50}$th of the length of the plate.

Calmon and Smith [6] use wire grid modelling to calculate the current on a surface. The fields close to the surface are then determined. The wire grid used by the authors is in the order of 0,1 λ in size. The authors found that with care the near field can be calculated as close as one grid spacing away from the surface.

Jambrina and Andres [7] show predicted and measured results of a twin fan antenna and monopole centered on top of a conducting box over an infinite groundplane. The size of the boxes used was of the same order of those of the antennas considered. According to the article the distances between parallel wires of the mesh were kept to less than a quarter wavelength. From the figure supplied in the article it looks as if more parallel wires were used. The radii were chosen so that the total wire surface was twice that of the original surface. Reasonable results were obtained by them.

Kubina and Larose [8] did a study where they modelled a dipole near a mast built of tubular segments. Predictions were done using both wires with the Method of Moments (NEC2) and four flat plates with the Geometrical Theory of Diffraction (GTD). Very similar results were obtained with both methods. A maximum segment length of 0.2 λ was used in the Method of Moment study.

Woodman and Stemp [9] discuss physical modelling of shipborne antennas. The factors that must be used in electromagnetic scale modelling of antennas are shown. The most important changes that must be made are the change of physical sizes, frequency and the conductance of all materials.

Newman et.al [10] give a technique for realistic modelling of arbitrary structures with polygonal patches. After a short introduction, details of the treatment of touching plates with overlapping patches are given. Three examples of scattering solutions are given namely a rocket, the Concorde aircraft and the Boeing 747 aircraft. It should be noted that the frequency used is low, such that the rocket is 2,4 λ long, the Concorde 1,8 λ and the Boeing 747 1,3 λ.

Rockway and Du Brul [11] state in their overview of shipboard antenna system predictions the following two basic facts. Firstly, no rigorous algorithms can be developed for selecting antenna locations until all the factors influencing the desirability of an antenna site have been identified and their influence on the system associated with the candidate antenna determined. Furthermore all factors influencing antenna site desirability cannot be determined until all antennas are located. The two basic facts are incompatible and can only be solved simultaneously using some iterative technique. They further made a comparison between the use of numerical modelling and physical modelling. The conclusion is reached that the two techniques are complementary. The direct cost for the numerical modelling relative to physical modelling was greater because of the cost of computer time, while the manpower cost was considerably lower.

Ludwig [25] examined the modelling of surfaces with a wire grid. He recognized that the results obtained using a wire grid model of a solid surface are sensitive to the wire diameter. He then examined the problem of wire grid modelling using an infinite long cylinder. Exact results for both the true problem and the wire grid model were used. This isolated the effects of wire grid modelling from other effects of the Method of Moments. He comes to the conclusion that the best accuracy is obtained when the wire diameter satifies the 'same surface area' rule of thumb. The effect of too thick wires is just as bad as too thin wires. He also shows that the boundary value match between wires is not a reliable check on the validity of far-field results.

1.4 Prediction methods used

Various methods to predict the performance of antennas on ships are available. The following four methods and variations of them are the best known.

1.4.1 Model measurement

Model measurement as applied to antennas on ships is a technique by which the radiating characteristics of physically large structures (such as an antenna on a ship) are determined by doing antenna measurements on suitably dimensioned scale models.

The scale normally used is 1/48, and this means that a frequency of 30 MHz is scaled to a frequency of 1 440 MHz. Because of the high frequencies encountered, the highest frequency band modelled is usually the HF band, although some modelling has taken place in the UHF band [12].

The main disadvantage of this technique is the high initial cost of building a accurate model of the ship. It is also very difficult to model any non-conducting part such as parts made of dielectric or magnetic materials (eg. composite materials such as carbon fibre and fibreglass). To be able to model such materials a very large range of materials with different dielectric and magnetic constants must be available. It is believed that more composite materials will be used in future in the ship building process.

Another major problem is the timescales needed to complete such a model. The model needs to include all the detail of the original ship and the surface finish needs to be of a comparable standard (taking the scale factor into account) to the real ship. It is furthermore quite difficult and expensive to make any major changes to the ship's structure after initial construction of the model.

An advantage of model measurements is the fact that once a model has been built up, a large number of measurements can be done in a fairly short time. This is possible because of automated measurement techniques. To do the scale measurements a properly developed antenna measurement facility must be available. Such a facility needs to be able to operate over a large frequency range. Measurements must also be done on a large groundplane.

1.4.2 Method of Moments (MM)

Electromagnetic radiation (or scattering) problems can always be represented by an integral equation. This equation can only be solved rigorously in a few special cases. The Method of Moments involves the reduction of the associated integral equation to a system of linear algebraic equations. The unknowns of this system are coefficients in some appropriate expansion of the current. By solving the resulting matrix equation, the currents on the structure can be computed. From the currents secondary parameters such as far fields, near fields, impedances and coupling can be obtained.

The number of simultaneous equations to be solved is directly related to the total size of the structure and the frequency. This means that for larger structures more equations are needed, while more equations follow at higher frequencies. This leads to the main disadvantage of this technique, namely that the amount of equations needed to be solved becomes larger than can be solved in a reasonable time and at a reasonable cost.

1.4.3 Geometrical Theory of Diffraction (GTD)

The Geometrical Theory of Diffraction is used where the wavelength used is much smaller than the structure under investigation. It is then possible to describe the electromagnetic wave interaction as optical rays, bouncing between scattering points. The basic scattering mechanisms at these points are diffraction and reflection. The interaction between a source and an observer is determined by adding contributions from all the possible ray paths and mechanisms between the two.

The time needed for a GTD solution is not determined by the size of the structure but by the number of possible rays that must be traced. This means that large structures can be analysed quite easily if the number of ray paths for the structure is small. This is usually true for large bodies that have no concave surfaces. GTD does not require a large memory. The main limitation of the GTD is that for all diffraction coefficients to be valid, all reflection/diffraction and source points as well as all geometrical dimensions must be in the order of at least one wavelength apart. This may be relaxed to a quarter wavelength for engineering purposes.

1.4.4 Hybrid methods

Because of the limitations of the Method of Moments and the GTD several types of hybrid methods were developed. Two such methods are described briefly below.

The GTD/MM hybrid method is one such method. The Method of Moments is used to determine diffraction coefficients which are used in the GTD solution. This method is mostly used in the analysis of antennas where the diffraction coefficients of certain structures are not known. An example of this method is found in the work done at Ohio State University on the radiation patterns of aperture matched horns [13].

The MM/GTD hybrid method is another class of hybrid methods. In this case a Method of Moments solution is set up for the antennas and their immediate neighborhood. In a true MM/GTD hybrid method the resulting interaction matrix is then modified by adding the contributions of reflections and/or diffractions from far-off (but still in the near-field) structures. This procedure results in a reduced matrix (thus less storage needed) and in most cases in reduced computation time.

In a simple MM/GTD method the currents of just the antenna and its immediate surrounding will be computed assuming that the rest of the structure does not exist. The currents of this area will then be used to obtain the far fields of the antenna in the presence of the whole structure. This method makes the assumption that the currents on the antenna are not affected by the structure. An example of this method is when a small wire antenna such as a ultra high frequency (UHF) yagi is mounted on a large structure such as a building.

2 THE METHOD OF MOMENTS

2.1 Introduction

The Method of Moments is a method whereby the radiation or scattering structure considered is divided in smaller sections (usually called segments or modes). The electromagnetic interactions between these sections are then computed as an impedance matrix. A voltage vector is set up according to the excitation field. Thus the problem is reduced to an equivalent set of simultaneous equations. This set of simultaneous equations is then solved to obtain the current on the structure. From the currents secondary parameters such as impedance, coupling and radiation patterns can be derived.

For the purpose of this discussion we limit ourselves to radiation and scattering from conducting structures.

2.2 Moment Methods

From Maxwell's equations we can derive a linear integral equation. Appendix A shows an example of such an integral equation.

Following the procedure in [2] the following is a introduction to the Moment Method.

Consider the inhomogeneous equation

$$L_{op}\Phi = \Gamma \tag{2.1}$$

where

L_ω is a linear operator,

Γ a known function and

Φ a function to be determined.

In the case of electromagnetic problems L_ω is normally an integral or integro-differential operator, Φ is the distribution of electrical current and Γ the impressed field or the applied voltage. Φ and Γ are both functions of the spatial coordinates and of the frequency.

The current distribution Φ can now be expressed in terms of known functions using undetermined parameters, for example, as a linear combination of a finite number of basis or expansion functions ϕ_j in the domain of L_ω thus

$$\Phi = \sum_j \alpha_j \phi_j \tag{2.2}$$

The constants α_j, which are finite in number, must now be determined. By substituting (2.2) into (2.1) we get

$$L_\omega\left(\sum_j \alpha_j \phi_j\right) = \Gamma \tag{2.3}$$

which for a linear operator leads to

$$\sum_j \alpha_j L_\omega(\phi_j) = \Gamma \tag{2.4}$$

Define a suitable inner product <a,b> for the problem in terms of an integral over the space S (for example the surface of a conducting body) for which the current distribution Φ is defined

$$<a,b> = \int_S (ab)\, ds \tag{2.5}$$

Define also a set of weighting functions w_i, in the range of the operator L_ω, and take the inner product of (2.4) with each w_i to get

$$\sum_j \alpha_j < w_i, L_\omega \phi_j > = < w_i, \Gamma >, \text{ for all i.} \tag{2.6}$$

The problem has thus been reduced to that of a set of linear algebraic equations which can be written in matrix notation as

$$\underline{L}\underline{\alpha} = \underline{\gamma} \tag{2.7}$$

where

$$\underline{L} = \begin{pmatrix} l_{11} & l_{12} & \cdot \\ l_{21} & l_{22} & \cdot \\ \cdot & \cdot & \cdot \end{pmatrix} \tag{2.8}$$

with

$$l_{nm} = < w_n, L_\omega \phi_m >$$

$$\underline{\alpha} = \begin{pmatrix} \alpha_1 \\ \alpha_2 \\ . \end{pmatrix} \tag{2.9}$$

$$\underline{\gamma} = \begin{pmatrix} \gamma_1 \\ \gamma_2 \\ . \end{pmatrix} \tag{2.10}$$

with

$\gamma_n = \langle w_2, \Gamma \rangle$

Equation (2.7) can be solved using any of the standard methods such as factorization of the $\underline{L}$ matrix.

The accuracy and efficiency of the method depends to a large scale on the choice of the basis functions ϕ_j and weighting functions w_j. Normally the basis and weighting function is chosen such that each is only non-zero over a region small compared to the wavelength. By using many such functions over the body, a body of arbitrary shape can be constructed independently of the specific basis functions.

2.3 Program NEC2.

The NEC2 program [14, 15, 16] is a computer code used to solve for the currents on thin wires or closed surfaces. In this study only the thin wire modelling capability of NEC2 is used, and no detail of the surface modelling is given.

The integral equation used by NEC2 is an electric-field integral equation (EFIE) which follows from an integral representation for the electric field of a volume current distribution $\overline{J}$:

$$\overline{E}(\overline{r}) = \frac{-j\eta}{4\pi k}\int_{v}\overline{J}(\overline{r}') \cdot \overline{\overline{G}}(\overline{r},\overline{r}')dV' \tag{2.11}$$

where

$$\overline{\overline{G}}(\overline{r},\overline{r}') = (k^2\overline{\overline{I}} + \Delta\Delta)g(\overline{r},\overline{r}')$$

$$g(\overline{r},\overline{r}') = \frac{e^{-jk|\overline{r}-\overline{r}'|}}{|\overline{r}-\overline{r}'|}$$

$$k = \omega\sqrt{\mu_0\varepsilon_0}$$

$$\eta = \sqrt{\frac{\mu_0}{\varepsilon_0}}$$

using the time convention $e^{j\omega t}$. $\overline{\overline{I}}$ is the identity dyad $(\hat{x}\hat{x} + \hat{y}\hat{y} + \hat{z}\hat{z})$.

If we consider a perfectly conducting body with the current distribution limited to the surface of the body, equation (2.11) becomes

$$\overline{E}(\overline{r}) = \frac{-j\eta}{4\pi k}\int_{S}\overline{J}_s(\overline{r}') \cdot \overline{\overline{G}}(\overline{r},\overline{r}')dA' \tag{2.12}$$

with $\overline{J}_s$ the surface current density. The observation point $\overline{r}$ is restricted to be off the surface S so that $\overline{r} \neq \overline{r}'$ or else $g(\overline{r},\overline{r}')$ becomes unbounded.

If $\overline{r}$ approaches S as a limit, equation 2.12 becomes

$$\overline{E}(\overline{r}) = \frac{-j\eta}{4\pi k}\int_s^p \overline{J}_s(\overline{r}')\cdot\overline{\overline{G}}(\overline{r},\overline{r}')dA' \tag{2.13}$$

where $\int^p$ indicates the principal value integral, since the integrand is unbounded.

The boundary condition for $\overline{r}\in S$ is

$$\hat{n}(\overline{r})\times[\overline{E}^s(\overline{r})+\overline{E}^i(\overline{r})]=0 \tag{2.14}$$

where $\hat{n}(\overline{r})$ is the unit normal vector of the surface at $\overline{r}$ and is the field due to the induced current $\overline{J}_s$.

Substituting equation 2.13 for $\overline{E}^s$ in (2.14) yields the integral equation

$$-\hat{n}(\overline{r})\times\overline{E}^i(\overline{r})=\frac{-j\eta}{4\pi k}\hat{n}(\overline{r})\times\int_s^p \overline{J}_s(\overline{r}')\cdot(k^2\overline{\overline{I}}+\Delta\Delta)g(\overline{r},\overline{r}')dA' \tag{2.15}$$

If the conducting surface S is that of a cylindrical thin wire, the vector integral in (2.15) can be reduced to a scalar integral equation. The assumptions applied for the thin wire are as follows:

1. All currents on the wire are assumed to flow in the axial direction.
2. There is no circumferential variation in the axial current.
3. The current is represented by a filament on the wire axis.
4. The boundary condition on the electric field is enforced in the axial direction only.

This set of approximations is valid as long as the wire radius is much less than the wavelength and much less than the wire length.

Using the first three assumptions, the surface current $\overline{J}_s(\overline{r})$ on a wire of radius a can be replaced by a filamentary current I where

$$I(s)\hat{s} = 2\pi a \overline{J}_s(\overline{r})$$

with

s = distance parameter along the wire axis at $\overline{r}$ and

$\hat{s}$ = unit vector tangent to the wire axis at $\overline{r}$.

Equation 2.15 then becomes

$$-\hat{n}(\overline{r}) \times \overline{E}^I(\overline{r}) = \frac{-j\eta}{4\pi k}\hat{n}(\overline{r}) \times \int_L I(s')\left(k^2\hat{s}' - \Delta\frac{\delta}{\delta s'}\right)g(\overline{r},\overline{r}')ds' \qquad (2.16)$$

where the integration is over the length of the wire. Enforcing the boundary condition in the axial direction reduces equation 2.16 to the scalar equation

$$-\hat{s} \cdot \overline{E}^I(\overline{r}) = \frac{-j\eta}{4\pi k}\int_L I(s')\left(k^2\hat{s} \cdot \hat{s}' - \frac{\delta^2}{\delta s\,\delta s'}\right)g(\overline{r},\overline{r}')ds' \qquad (2.17)$$

$\overline{r}'$ is now the point at s' on the wire axis while $\overline{r}$ is a point at s on the wire surface and thus $|\overline{r} - \overline{r}'| \geq a$ and the integrand is bounded.

Wires in NEC2 are modelled by short straight segments with the current on each segment represented by three terms, a constant, a sine and a cosine. This type of current has the advantage that the fields of the sinusoidal currents are easily evaluated in closed form. The amplitudes of the constant, sine and cosine terms are related such that their sum satisfies physical conditions on the local behavior of current and charge at the segment ends.

The total current on segment number j in NEC2 has the form

$$I_j(s) = A_j + B_j \sin k(s - s_j) + C_j \cos k(s - s_j) \qquad (2.18)$$

where

$|s - s_j| < \Delta_j/2$

where s_j the value of s at the center of segment j and Δ_j the length of segment j is.

Of the three unknown constants A, B and C, two are eliminated by local conditions on the current leaving one constant, related to the current magnitude, to be determined by the matrix equation.

The local conditions are applied to the current and to the linear charge density, q, which is related to the current by the equation of continuity

$$\frac{\delta I}{\delta s} = -j\omega q \qquad (2.19)$$

The current and charge are always such that current and charge are continuous at a junction, and that current goes to approximately zero at wire ends. For the details of the implementation the NEC2 manuals are referenced.

The results of applying the basis functions is that the current is a peak in the segment where it is defined, and goes to zero with a zero derivative at the far end of adjacent segments as shown in figure 2.1.

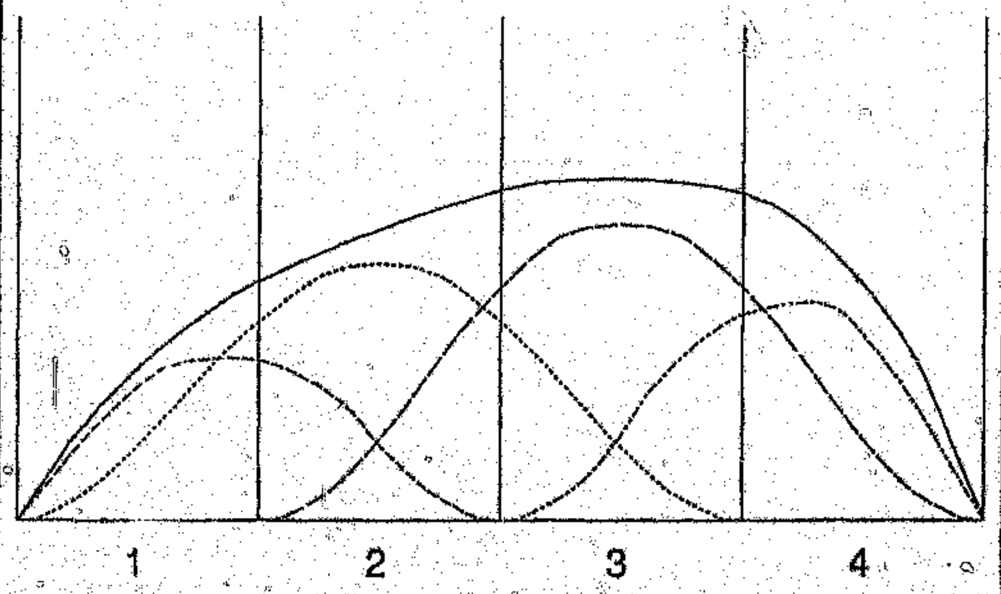

Figure 2.1 Basis function used in NEC2.

A model may include nonradiating networks and transmission lines connecting different parts of the structure, perfect or imperfect conductors, and lumped element loading. A perfectly or imperfectly conducting groundplane may also be placed in the model.

NEC2 includes several different source models. The simplest of this is the incident plane wave on the structure. This can be used for modelling receiving antennas where the current at the feedpoint is required. It is also used for EMP studies where induced currents on the structure are calculated. An incident plane wave is also used in scattering studies where the field scattered by the structure is examined. This is not very useful in the present study and no further details are given here.

A useful source model and the one mostly used in NEC2 is the applied electric field model. Here an electric field is specified at a single match point. For a voltage source of strength V on segment i, the element in the excitation vector corresponding to the applied electric field at the center of segment i is set to

$$E_i = \frac{V}{\Delta_i} \tag{2.20}$$

where Δ_i is the length of segment i. The direction of E_i is toward the positive end of the voltage source so that charge is pushed in the same direction as the source. The field at other match points is set to zero.

The actual effective voltage is the line integral of the applied field along the wire. This field is not known a priori but may be determined after the current is found by integrating the scattered field produced by the current. The field is nearly constant over the segment and drops sharply at the segment ends. This means that the approximation of the voltage in equation (2.20) above is approximately correct.

The antenna input impedance is computed by dividing the current at the centre of the segment (assuming it to be the average current) by the applied voltage. If the segment is short and a symmetric feedpoint is used so that the current of the center equals the average current and the assumed voltage equals the actual applied voltage, fairly accurate admittance results can be obtained.

Another source model is the current-slope discontinuity model which is based on a discontinuity in the derivative of current. For this model the source region is viewed as a biconical transmission line with feed point at the source location as shown in figure 2.2. The voltage between a point at s and the symmetric point on the other side of the line is then related to the derivative of the current by the transmission line equation

$$V(s) = -jZ_0 \frac{\partial I(ks)}{\partial(ks)} \tag{2.21}$$

where Z_0 the characteristic impedance of the transmission line is.

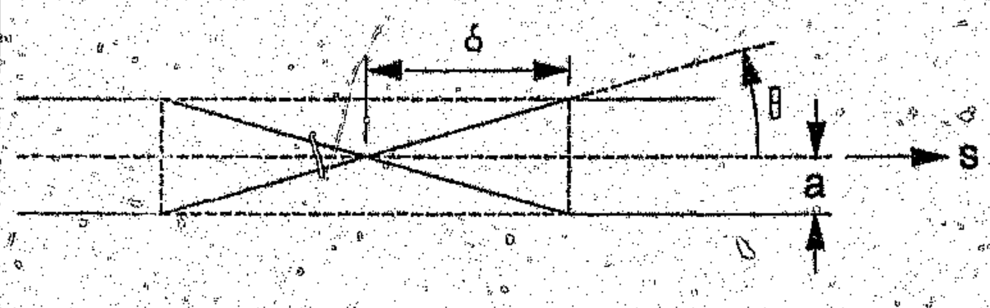

Figure 2.2 Biconical Transmission Line Model of Source Region.

By taking the known transmission line impedance equation we can obtain the relationship between the voltage V_0 of a source at s_0 and the discontinuity in current derivative as

$$\lim_{\varepsilon \to 0}\left[\left.\frac{\partial I(ks)}{\partial(ks)}\right|_{s=s_0+\varepsilon} - \left.\frac{\partial I(ks)}{\partial(ks)}\right|_{s=s_0-\varepsilon} \right] = \frac{-jV_0}{60\left[\ln\left(\frac{2d}{a}\right) - 1\right]} \tag{2.22}$$

By making suitable changes to the basis functions the discontinuity in current can be introduced. For details of this procedure see [14].

With the current slope discontinuity model the admittance is the ratio of the current at the segment end, where the source is located, to the source voltage. The two segments on opposite sides of the source must have equal length and radii. This means that this model can not be used to model monopoles or to feed at the junction of more than one wire.

2.4 Program THWIRE.

The THWIRE program [17, 18] is a thin wire Method of Moments program used to calculate the currents on the wires because of a specified excitation. From the currents several secondary parameters such as input impedance, coupling between ports and radiation patterns may be computed.

The program uses the reaction integral equation as described in Appendix A.

The program makes use of similar basis and test functions and thus a symmetrical matrix is created. The basis and test functions are defined over what are called expansion or test dipoles. Each such dipole consists of two adjacent segments of the wire structure. Such a dipole can be a linear dipole (when the two segments form a straight line) or a V-dipole (when there is an angle other than 180° between the two segments).

The current distribution of a linear expansion or test dipole is shown in figure 2.3 and given by

$$\bar{I}(z) = \frac{\hat{z}P_1 \sinh\gamma(z - z_1)}{\sinh\gamma d_1} + \frac{\hat{z}P_2 \sinh\gamma(z_3 - z)}{\sinh\gamma d_2} \tag{2.23}$$

where

$P_1(z) = 1, z_1 < z < z_2$

$\quad 0, elsewhere$

$P_2(z) = 1, z_2 < z < z_3$

$\quad 0, elsewhere$

$d_1 = z_2 - z_1$

$d_2 = z_3 - z_2$

$\gamma = s\sqrt{\mu\varepsilon}$

For a V expansion or test dipole the current distribution is

$$\bar{I}(l) = \frac{\hat{l}_1 P_1 \sinh\gamma(l - l_1)}{\sinh\gamma d_1} + \frac{\hat{l}_2 P_2 \sinh\gamma(l_3 - l)}{\sinh\gamma d_2} \tag{2.24}$$

where l is the length parameter on the dipole.

For a feed model THWIRE uses a delta gap model where a terminal voltage is simply enforced on one of the dipoles.

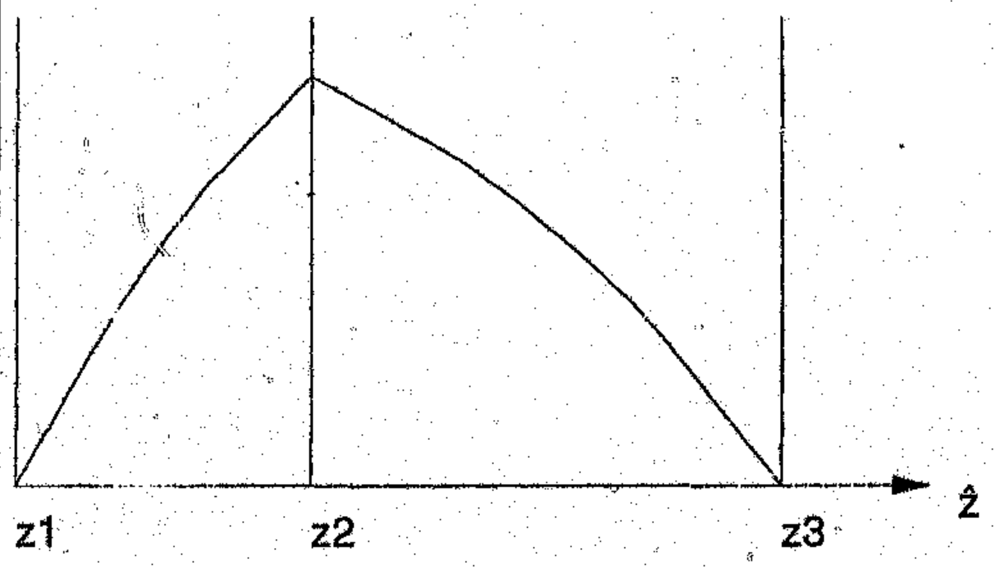

Figure 2.3 A linear expansion/test dipole used by THWIRE. The endpoints of the dipole are at z_1 and z_3 with terminals at z_2.

2.5 Program ESP.

The ESP program [19] is a Method of Moment program that make use of both thin wire structures and surface patches. The surface patches are two dimensional rectangular surfaces that support currents on the surface.

Three basic types of modes are used: wire dipole modes, surface dipole modes and a special attachment mode whenever a wire connects to a surface. With this choice of expansion functions geometries consisting of flat surfaces, thin wires and wire-surface connections may be modeled. A singly curved surface may be modelled using a piecewise flat approximation.

The wire mode used is similar to that used in THWIRE (see 2.4 above). It is a piecewise-sinusoidal V-dipole consisting of two sinusoidal monopoles. For a sketch of such a mode see figure 2.3. The current on this wire is given by

$$\overline{J}_z^w = \frac{\hat{z}}{2\pi a}\left[P_1 \frac{\sin k(z - z_1)}{\sin k(z_2 - z_1)} + P_2 \frac{\sin k(z_3 - z)}{\sin k(z_3 - z_2)} \right] \tag{2.25}$$

with

$P_1(z) = 1, z_1 < z < z_2$

$\quad 0, elsewhere$

$P_2(z) = 1, z_2 < z < z_3$

$\quad 0, elsewhere$

and a the wire radius.

These modes are placed in an overlapping array on the wire ensuring continuity of current on the wire.

The surface-patch mode is a surface V-dipole consisting of two sinusoidal surface monopoles. An example of a surface V-dipole with interior angle of 180° is shown in figure 2.4. The current on this dipole is given by

$$\overline{J}_s^s = \hat{z}\frac{kP_1 \sin k(z - z_1)\cos ky}{2\sin k(z_2 - z_1)\sin kw} + \hat{z}\frac{kP_2 \sin k(z_3 - z)\cos ky}{2\sin k(z_3 - z_2)\sin kw} \tag{2.26}$$

with

P_1, P_2 as above

w half the width of the dipole.

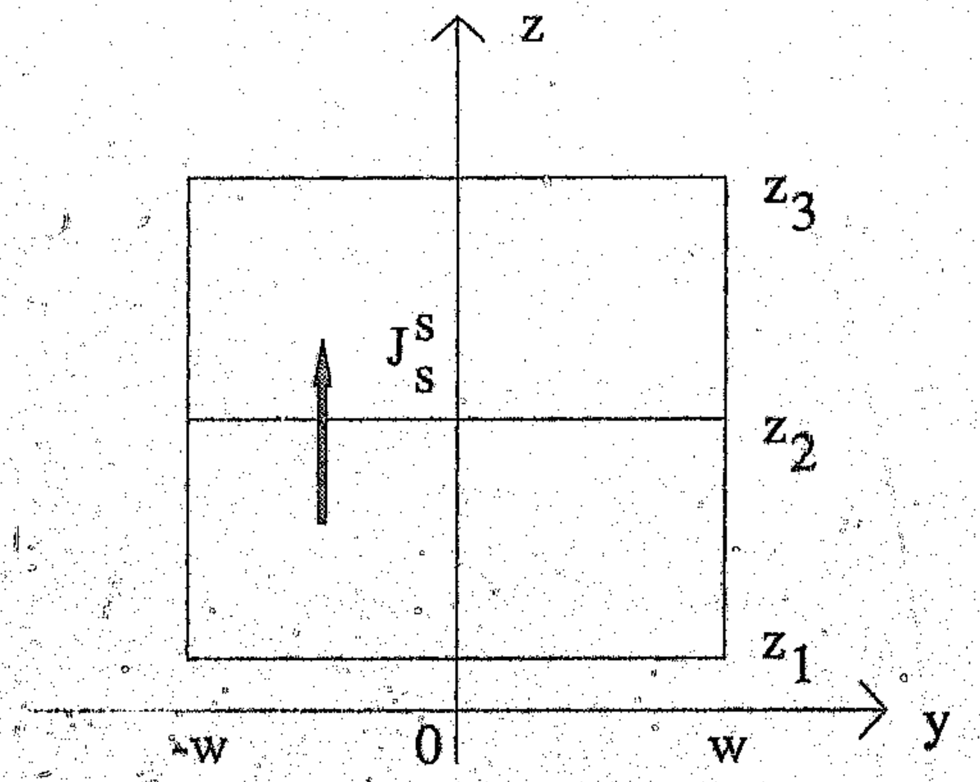

Figure 2.4 Sinusoidal surface V-dipole.

Two orthogonal and overlapping arrays of the surface patch modes are placed on the surface, allowing a two-dimensional vector surface current density.

Where a wire is attached to a surface, a special attachment mode is needed. This mode must insure both continuity of current at the junction and the proper $\hat{\rho}$ polarization and $\frac{1}{\rho}$ dependence of the current density close to the junction. This mode consists of two parts, a wire monopole and a disk monopole as shown in figure 2.5. The wire monopole current density is similar to that of a thin wire mode and is defined as

$$\overline{J}_s^w = \frac{\hat{z}}{2\pi a}\frac{\sin k(z_2 - z)}{\sin k z_2} \tag{2.27}$$

where the disk current density is defined as

$$\overline{J}_s^d = \frac{\hat{\rho}}{2\pi\rho}\frac{-\sin k(b-\rho)}{\sin k(b-a)} \tag{2.28}$$

where

a, b are the inner and outer radii of the disk.

Note that the inner radius of the disk is equal to the wire radius, that the current on the disk at a is equal to the current at z=0 on the wire to ensure continuity of current at the junction. The current on the disk at b is equal to zero to ensure continuity of current on the surface.

It is important to note that with these expansion functions the current is always continuous in the direction of the current, but it may not be continuous in the direction orthogonal to the current flow.

For antennas the same feed model is used as in THWIRE, that is, a delta gap model where a terminal voltage is simply enforced on one of the dipoles.

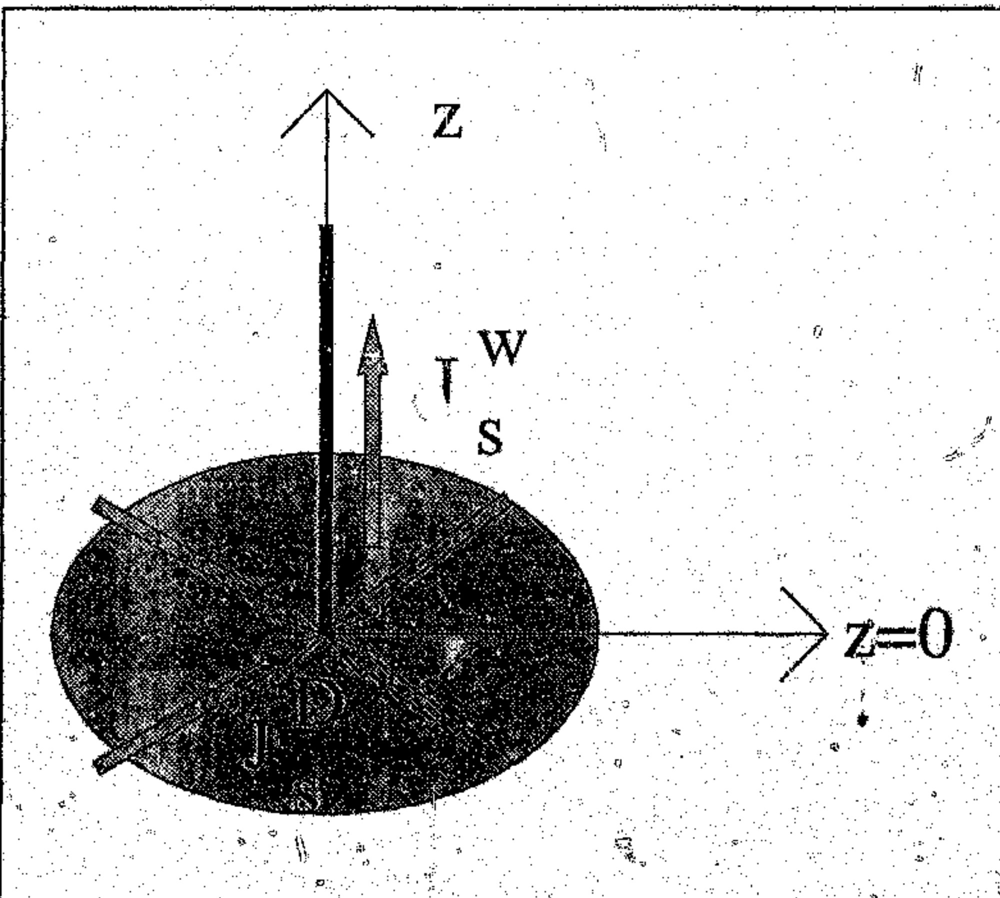

Figure 2.5 Attachment dipole mode.

2.6 Verifying the Method of Moments with dipoles

As a test case and to prove converge of the results from Method of Moment codes, a dipole antenna near resonance was analyzed. This antenna was 0.5m long and the frequencies used were between 290 and 310 MHz. The radius of the wire is 2 mm for all the cases.

Programs NEC2 and THWIRE were used in this part of the study. Because NEC2 gives several different options of feed models the differences between the applied E-field and the current discontinuity model were investigated (see the description of NEC2 for more information on the feed models). For the applied E-field model, the effect of keeping the feed segment at a fixed length or varying the length was investigated.

A summary of the results obtained using NEC2 and THWIRE are presented in graphical form in figures 2.6 to 2.9. These NEC2 results are all for the applied E-field feed model where the feed segment length was changed between the different cases to be the same length as that of the rest of the segments. These results are also tabulated in appendix C.

Figures 2.10 and 2.11 show the convergence of the impedance results with both NEC2 and THWIRE. For the NEC2 results the several different antenna models used are shown. This results are shown for a frequency of 300 MHz.

From the results it is clear that the applied E-field model of NEC2 gives very similar results to the THWIRE results. It can also be seen that a large number of segments are needed before the impedances converge. This shows the difficulty in computing impedance data because of the local nature of impedances.

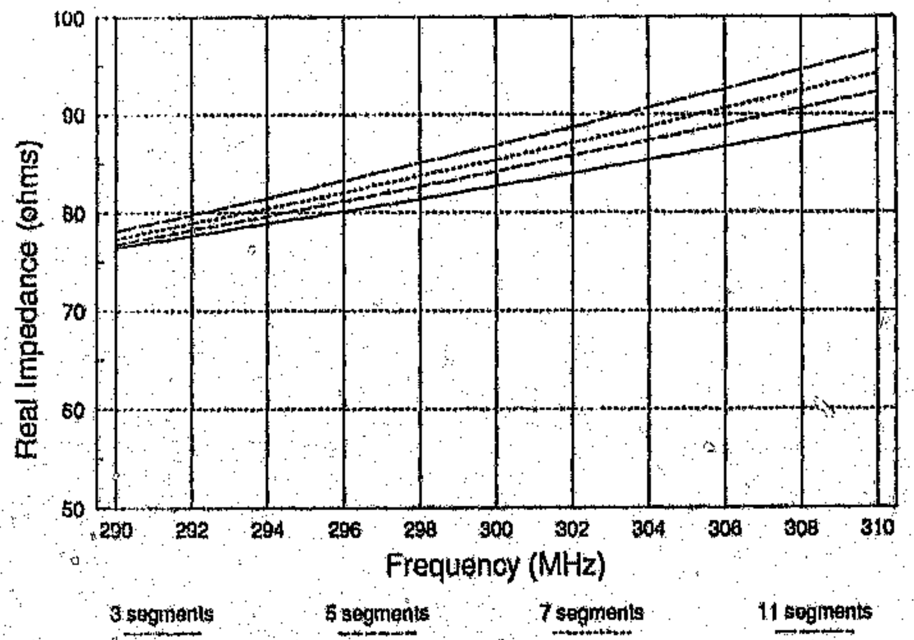

Figure 2.6 Real part of Impedance of dipole as computed by NEC2.

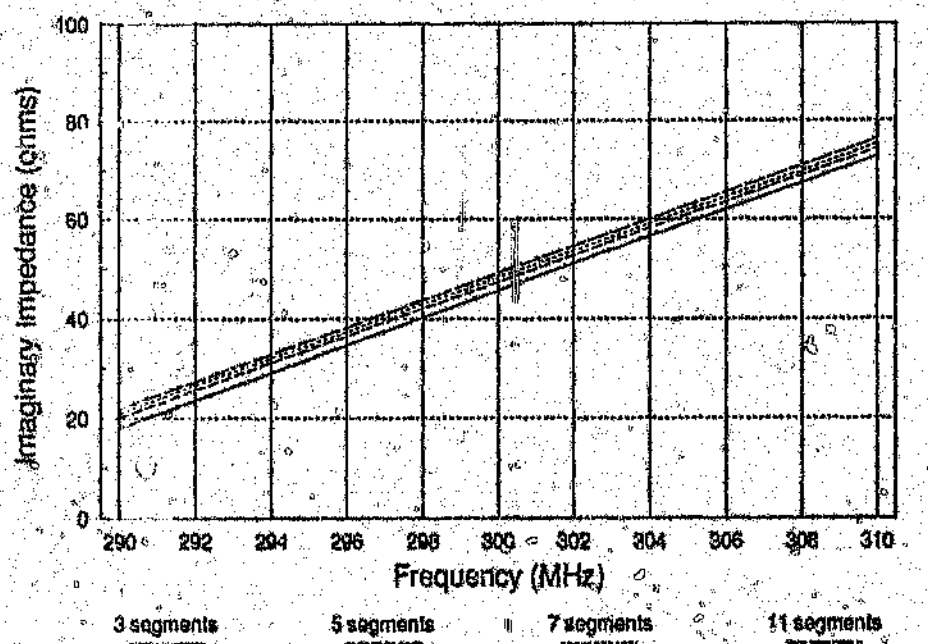

Figure 2.7 Imaginary part of impedance of dipole as computed by NEC2.

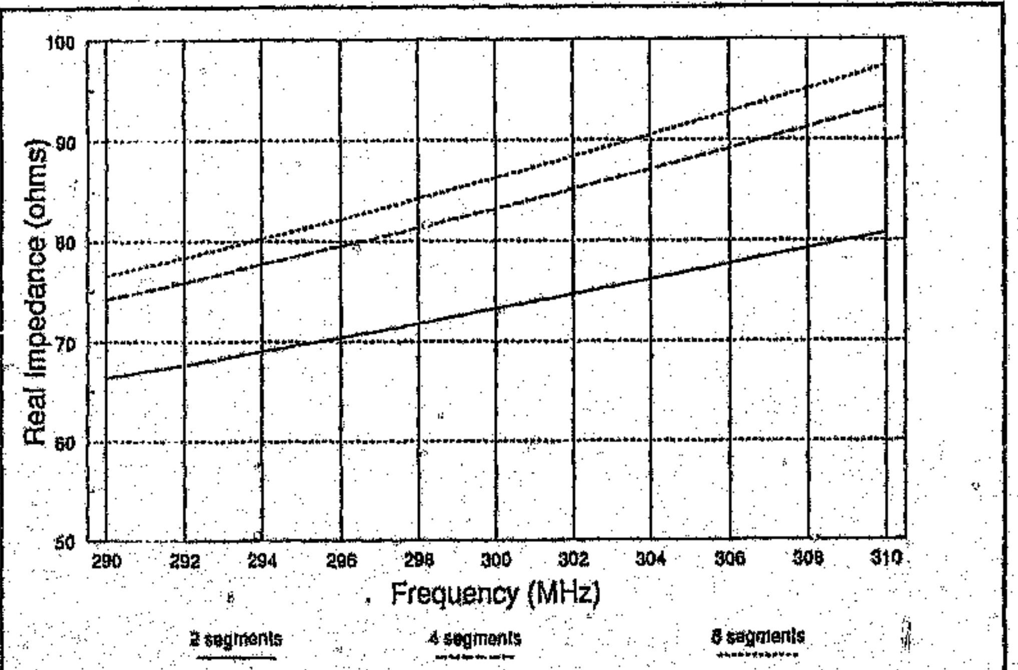

Figure 2.8 Real part of impedance of dipole as computed by THWIRE.

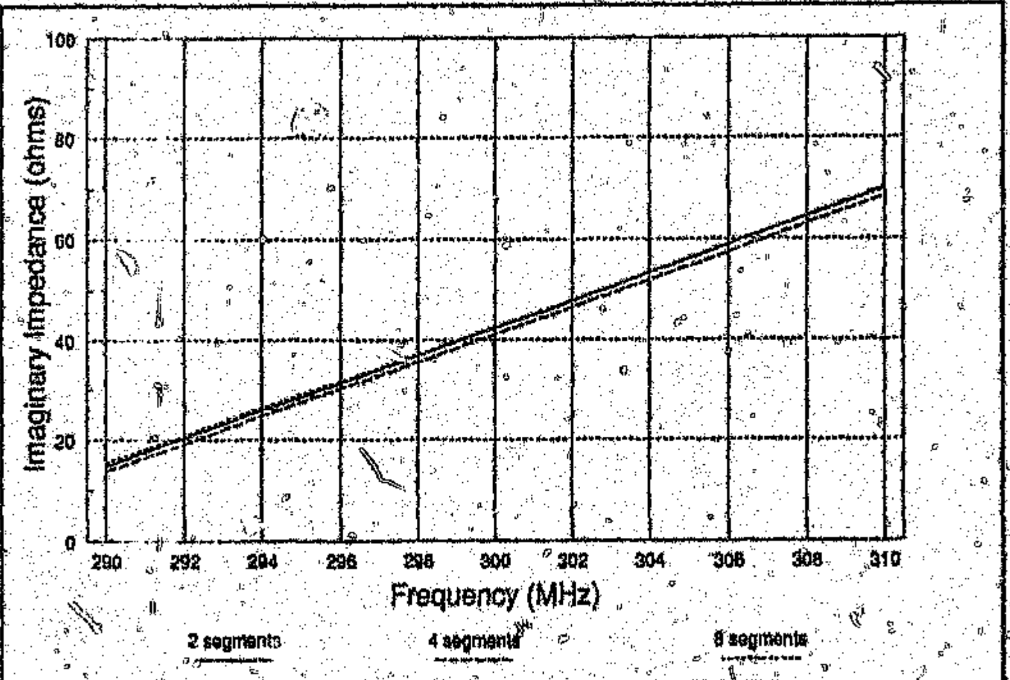

Figure 2.9 Imaginary part of impedance of dipole as computed by THWIRE.

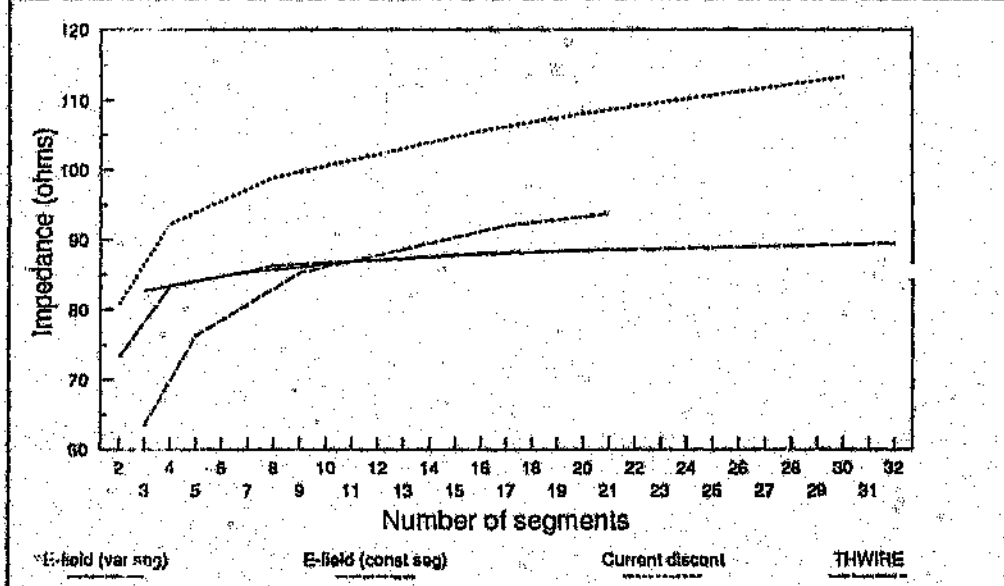

Figure 2.10 Convergence of the real p[illegible] of the impedance of a dipole with NEC2 and THWIRE.

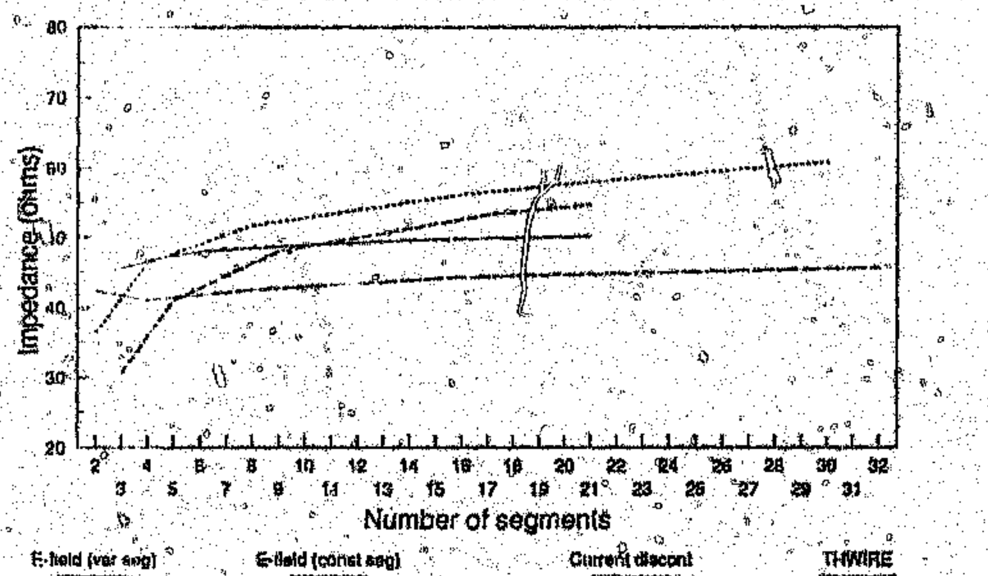

Figure 2.11 Convergence of the imaginary part of the impedance of a dipole with NEC2 and THWIRE.

2.7 Modelling Surface Structures

Solid surfaces can be modelled in the Method of Moments by using wire grids as shown in figures 2.12 and 2.13.

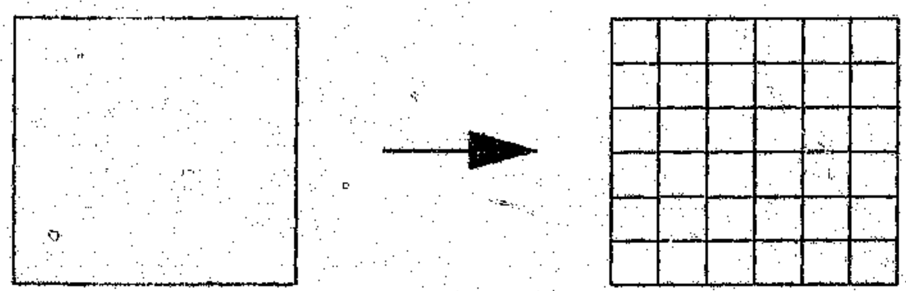

Figure 2.12 Example of a rectangular wire grid model of a surface.

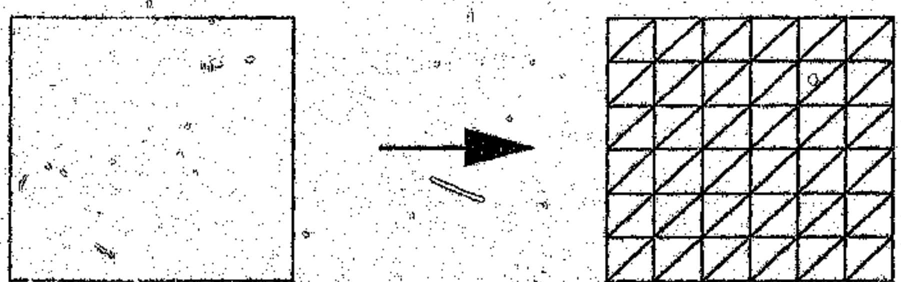

Figure 2.13 Example of a triangular wire grid model of a surface.

The mesh size must be small compared to the wavelength (0.02 - 0.03 square wavelengths)[2]. This size has been determined by numerical experiment. More wires must be used near edges and on places where the radius of curvature is small.

One of the main problems is that currents are forced to flow along wires. For this reason a triangular mesh might be better to use than a rectangular mesh. It is much more difficult to form a triangular mesh than it is to form a rectangular mesh. Should currents tend to flow in any particular direction then the wires in the mesh should be directed in that direction.

The radius of the wires should be such that the total surface area of the wires is twice the surface area of the modelled surface [2]. By experiment it was found that the wire surface should never be less than the modelled area. If the above statement is true, then for radar cross section (RCS) computations, the position of the RCS lobes will be correctly predicted and the magnitude of the major lobes will be correct. Major lobes are not very much affected by radius size. The wires should be of the same conductivity as the surface.

To test some of the above statements, a two meter square plate with a quarter meter monopole mounted on it was selected as a test vehicle. A frequency of 300 MHz was chosen as one wavelength is equal to one meter at this frequency. Several different options were tried to find a reliable method of modelling such a surface.

To determine the necessary radius required for a square grid, a grid size of 0.15m was chosen and computations done at different wire radii. Figure 2.14 shows the result for two radii. It was found that convergence was achieved at a radius of about 0.0227m. The same experiment was repeated for a grid size of 0.1m. Results for this case are shown in figure 2.15. From the two grid sizes the deduction was made that the wire surface must be equal to twice the surface of the modelled surface and corresponds to the following formula (see appendix D for the derivation).

$$a = d/2\pi \tag{2.29}$$

with a the wire radius and d the grid size (distance between two wires).

To determine the necessary grid size to use, a number of computations were done with different grid sizes. In all cases the radius was chosen using the formula above. Figure 2.16 shows the results for two grid sizes. It was found that convergence was achieved at a grid size of 0,1m, that is, 10 wires per wavelength.

A test on the grid size for a triangular grid was also done. The necessary wire radius is derived in appendix E. Figure 2.17 shows the results. In this case a wire length of 0,15m was found to be optimum. This result is compared with the previous result for the rectangular grid in figure 2.18 and the results are nearly identical.

All computations were done under the assumption that the plate was made from a perfectly conducting material. Figure 2.19 shows the comparison between a perfectly conducting plate and one of finite conductivity. No difference between the two plots can be seen.

The last and most difficult test was to compare the predicted results to measured results. This is done in figures 2.20 to 2.23 for a rectangular infinitely conducting grid and in figures 2.24 to 2.27 for a triangular finite conducting grid at a number of frequencies close to 300 MHz. In all cases the results compare within the typical measurement errors.

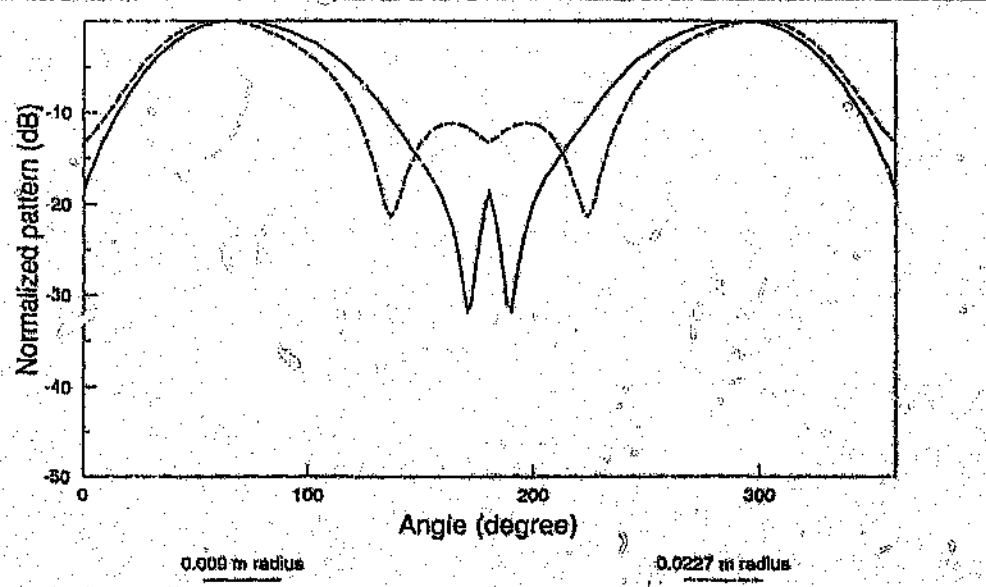

Figure 2.14 Comparison between the prediction of the 2 by 2 m square plate with a 0.15 m rectangular grid and a 0.009 m or a 0.0227 m wire radius. Frequency is 300 MHz.

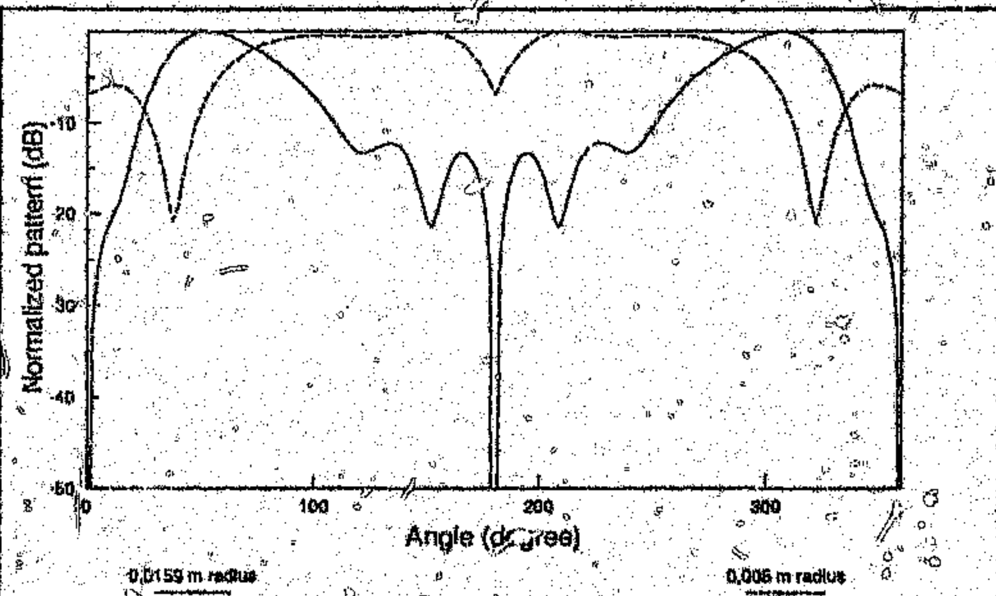

Figure 2.15 Comparison between the prediction of the 2 by 2 m square plate with a 0.1 m rectangular grid and a 0.005 m or a 0.0159 m wire radius. Frequency is 300 MHz.

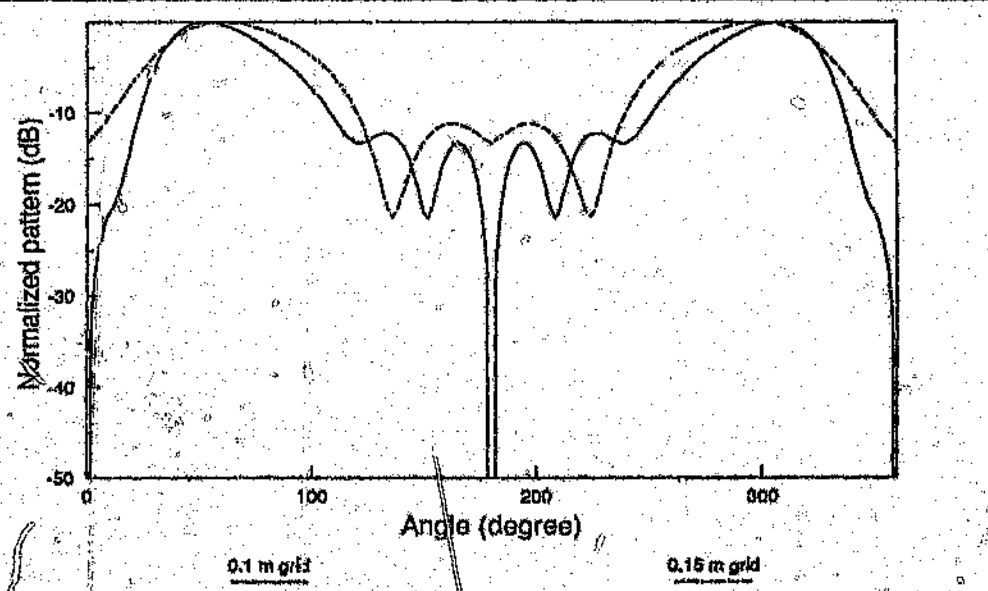

Figure 2.16 Comparison between the prediction of the 2 by 2 m square plate with a 0.1 or 0.15 m rectangular grid (0.0159/0.0227 m wire radius respectively). Frequency is 300 MHz.

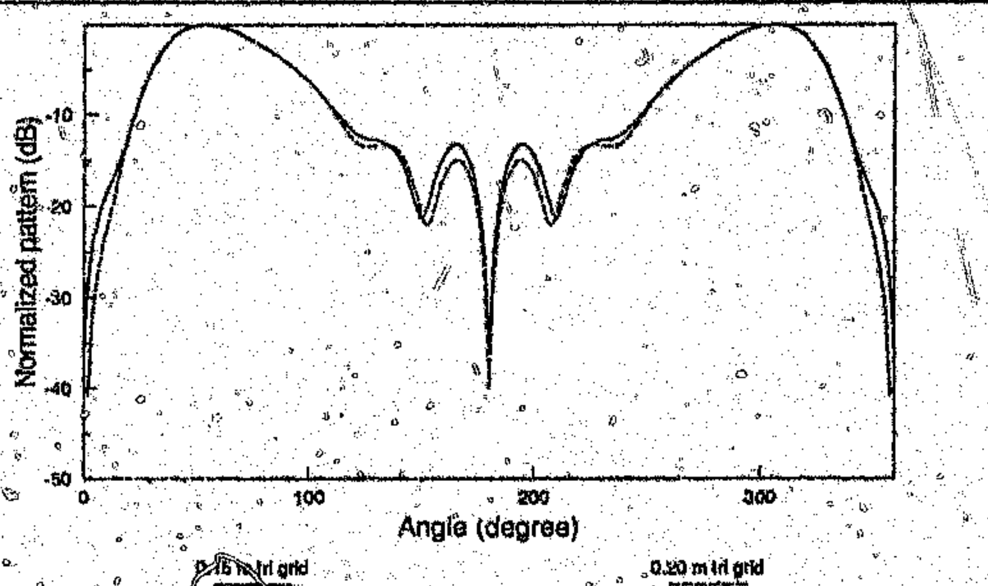

Figure 2.17 Comparison between the prediction of the 2 by 2 m square plate with a 0.15 or 0.20 m triangular grid (0.0159/0.02 m wire radius). Frequency is 300 MHz.

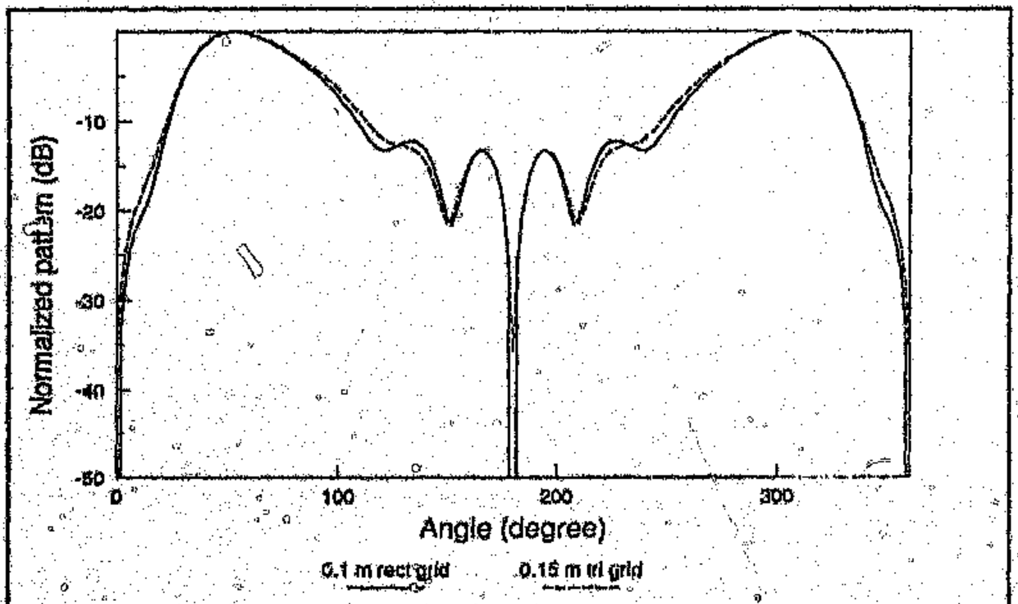

Figure 2.18 Comparison between the prediction of the 2 by 2 m square plate with a 0.1 m rectangular or 0.15 m triangular grid (0.0159 m wire radius). Frequency is 300 MHz.

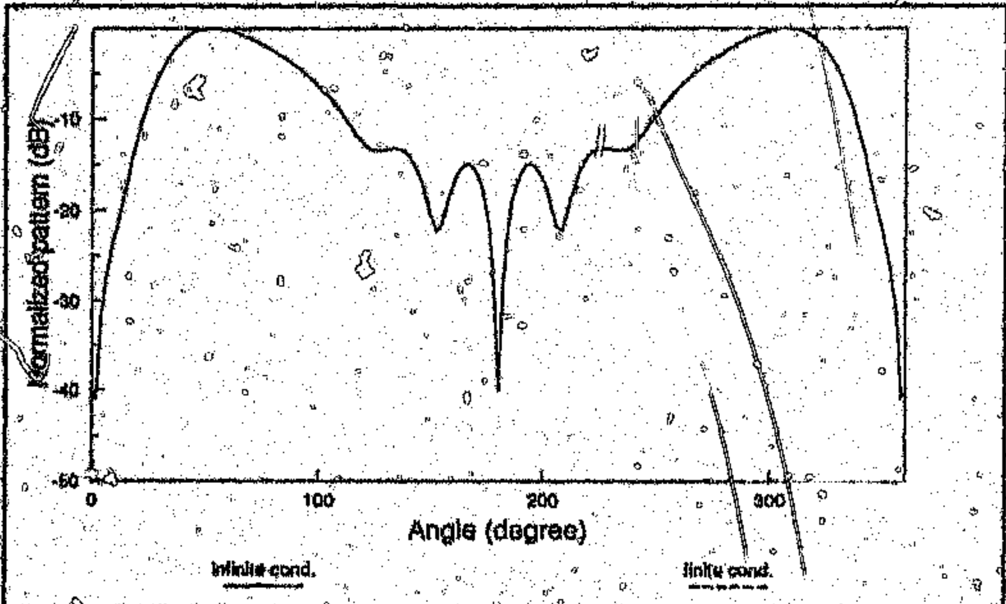

Figure 2.19 Comparison between the prediction of the 2 by 2 m square plate with a 0.2 m triangular grid and finite or infinite conductivity (0.02 m wire radius). Frequency is 300 MHz.

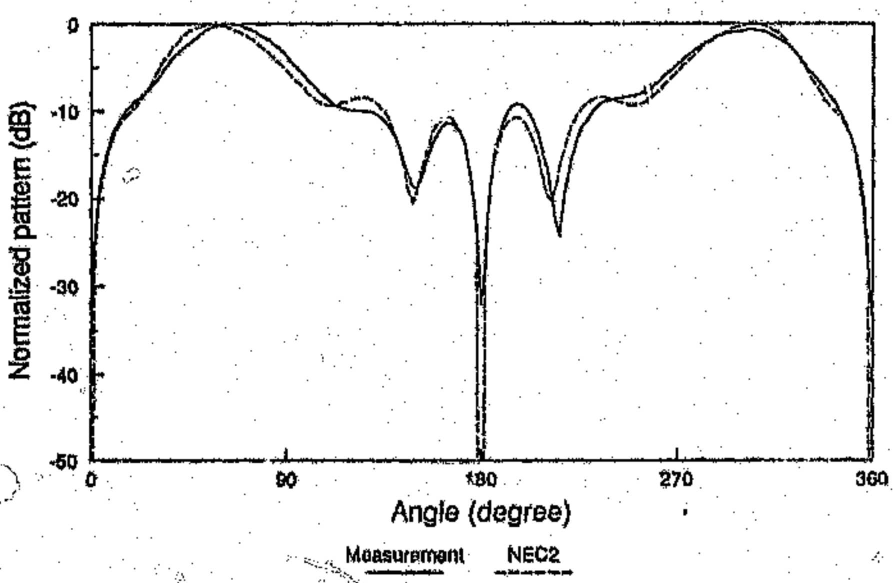

Figure 2.20 Comparison between the predictions and measurement (at 270 MHz) of the 2 by 2 m square plate (elevation plane, rectangular grid 0.1 m with 0.0159 m radius).

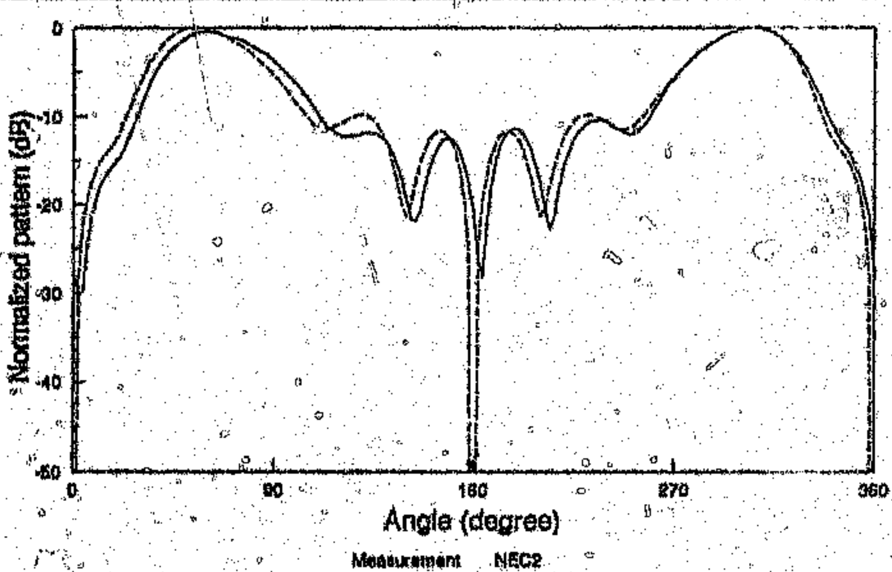

Figure 2.21 Comparison between the predictions and measurement (at 280 MHz) of the 2 by 2 m square plate (elevation plane, rectangular grid 0.1 m with 0.0159 m radius).

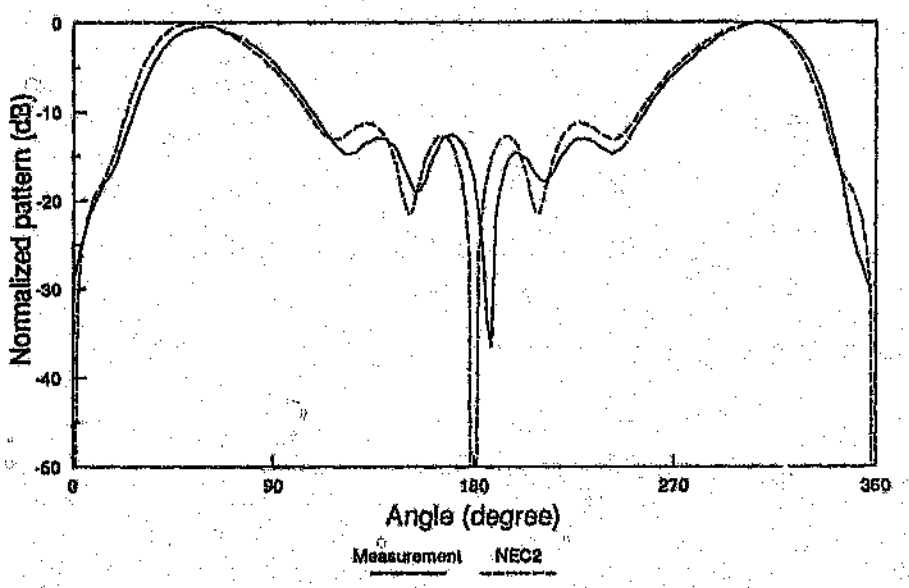

Figure 2.22 Comparison between the predictions and measurement (at 290 MHz) of the 2 by 2 m square plate (elevation plane, rectangular grid 0.1 m with 0.0159 m radius).

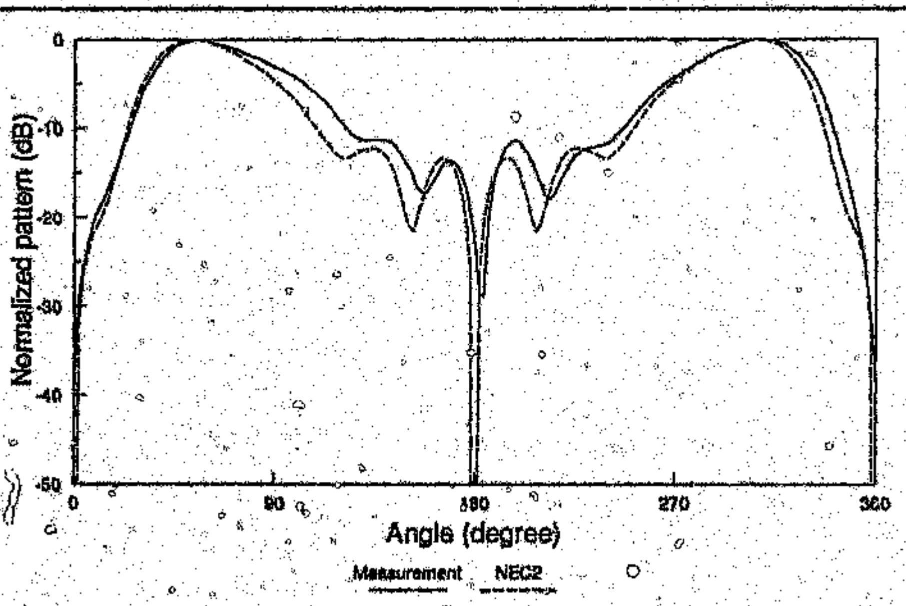

Figure 2.23 Comparison between the predictions and measurement (at 300 MHz) of the 2 by 2 m square plate (elevation plane, rectangular grid 0.1 m with 0.0159 m radius).

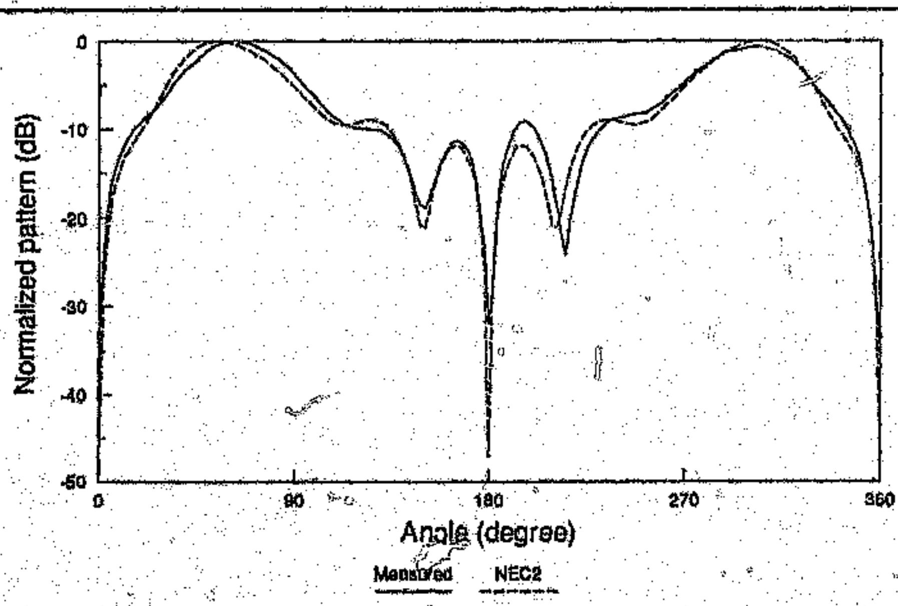

Figure 2.24 Comparison between the predictions and measurement (at 270 MHz) of the 2 by 2 m square plate (elevation plane, triangular grid 0.2 m with 0.02 m radius, finite conductivity).

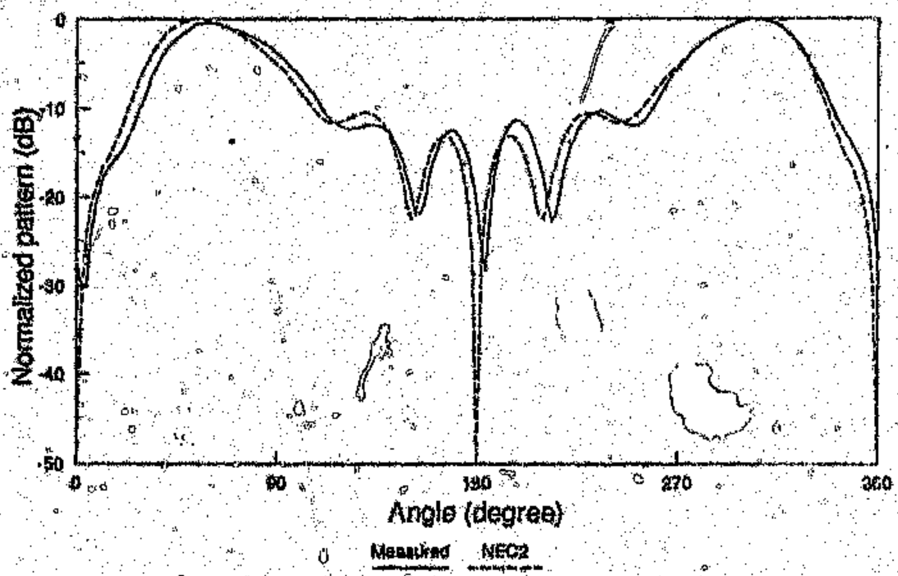

Figure 2.25 Comparison between the predictions and measurement (at 280 MHz) of the 2 by 2 m square plate (elevation plane, triangular grid 0.2 m with 0.02 m radius, finite conductivity).

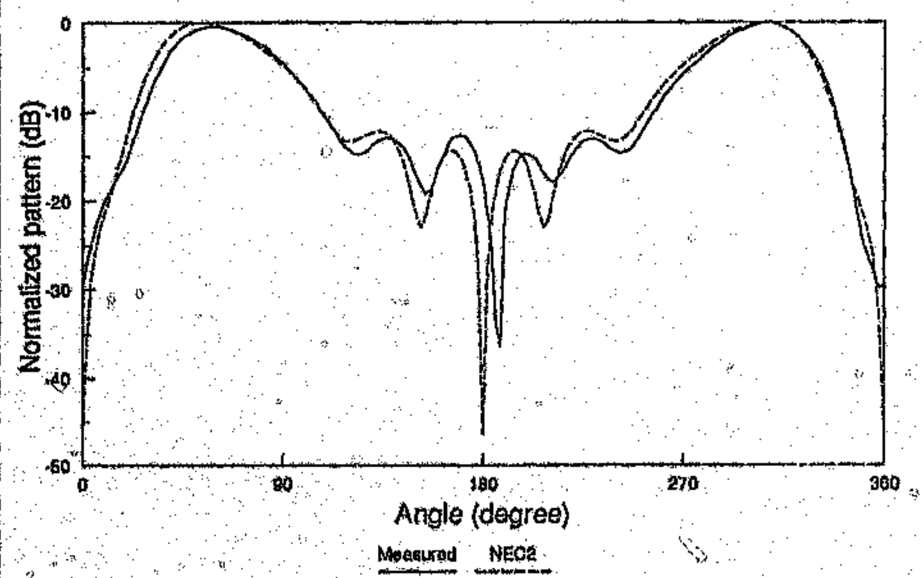

Figure 2.26 Comparison between the predictions and measurement (at 290 MHz) of the 2 by 2 m square plate (elevation plane, triangular grid 0.2 m with 0.02 m radius, finite conductivity).

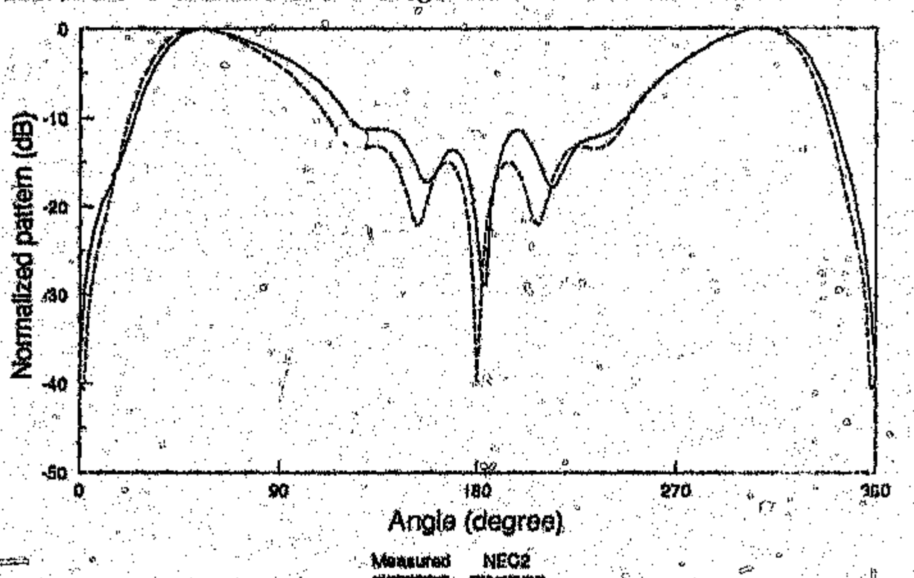

Figure 2.27 Comparison between the predictions and measurement (at 300 MHz) of the 2 by 2 m square plate (elevation plane, triangular grid 0.2 m with 0.02 m radius, finite conductivity).

2.8 Discussion

A short introduction into the Method of Moments was given. Several computer codes used by the author were described.

To verify the Method of Moments several impedance studies on a dipole were done. The best convergence of the impedance data was found using NEC2 with an applied E-field source model. The solutions were within a few percent of the final solution when about 20 segments per wavelength were used. It is concluded from the study that care must be taken when impedance calculations are made using the Method of Moments.

A study to determine the necessary grid spacing and wire radius for modelling surfaces with wire grids was performed. From the study it was concluded that there is no significant difference between a rectangular and a triangular mesh. It can furthermore be concluded that a wire grid size of a hundredth of a square wavelength is adequate for radiation pattern studies. This corresponds to a wire segment length of a [illegible] a wavelength for a rectangular grid. The radius of the wire must be such that the total surface of all the wires are equal to twice the surface of the plate being modelled. This means that for a rectangular grid, the radius must be 0,159 times the wire segment length and for a triangular grid 0,09 times the wire segment length.

3 RESULTS

3.1 Introduction.

The results obtained in the modelling of a ship are given in this chapter. This chapter shows the typical results that one would like to compute namely radiation patterns and currents. Because of the massive number of segments (modes) needed for a large structure such as a ship, the study is started with a greatly simplified model and the model is gradually increased in complexity.

3.2 Geometry of ship.

The geometry of the ship considered in this study is given in figure 3.1. Please note that this ship is actually a 1/250 model of a typical real ship, but the dimensions was chosen so that measurements could be made in an anechoic chamber. The scale was chosen such that a frequency of 1 GHz represents a frequency of 4.0 MHz in the HF band on the ship.

3.3 First model. (Model A)

A drawing of the first model is shown in figure 3.2. This model only includes the antenna platform and the vertical plate representing the first higher deck. The model was discretised for a maximum frequency of 4.0 GHz. A total of 409 segments are used in this model for the ship, with 4 segments used for each antenna represented on the ship.

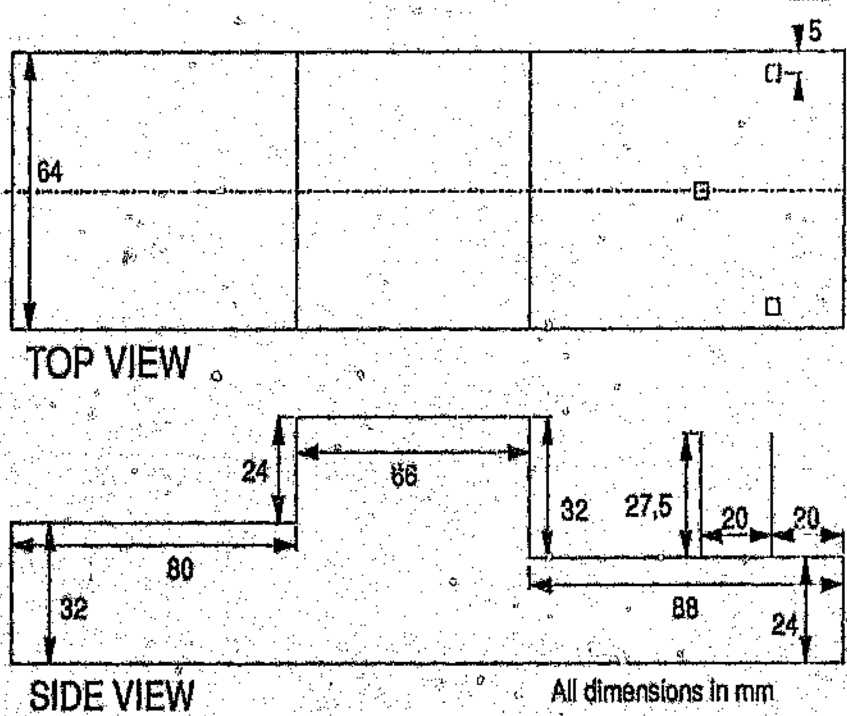

Figure 3.1 Geometry of the full ship model used in this study.

Figures 3.3 to 3.6 show the radiation pattern of the middle antenna of model A (with no other antenna connected) compared to measurements. As can be seen from the figures, the comparison of the pattern in the forward scattered area is relatively good (within 3 dB), but the backward pattern is not so good. This was expected as the model is not very accurate to the back. The patterns are better at the higher than at the lower frequencies. This may indicate that the currents are more concentrated closer to the antennas at the higher frequencies. This is because the structure is electromagneticly so much larger at higher frequencies.

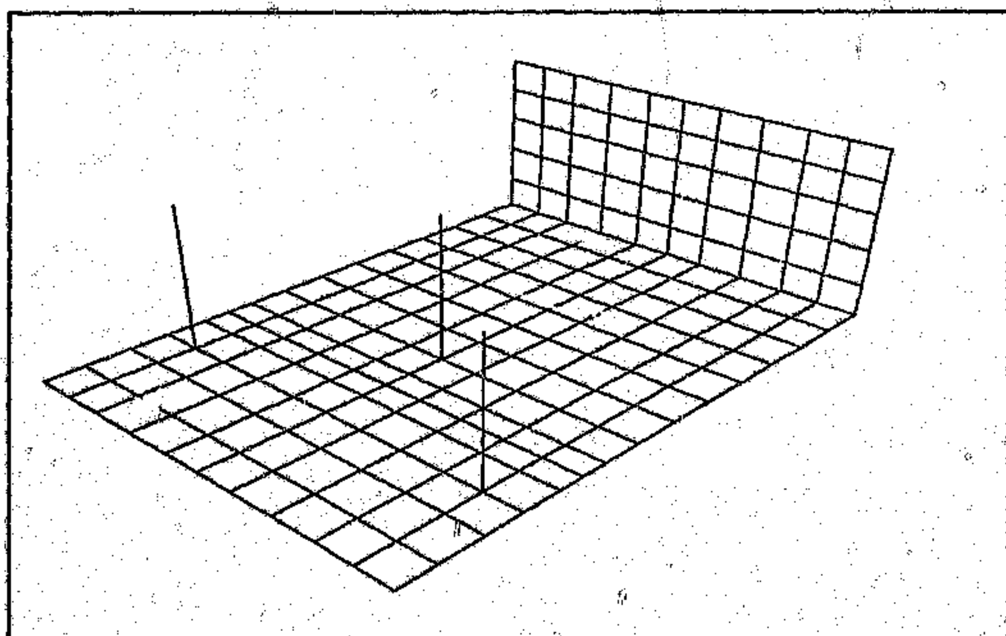

Figure 3.2 Discretised ship for model A.

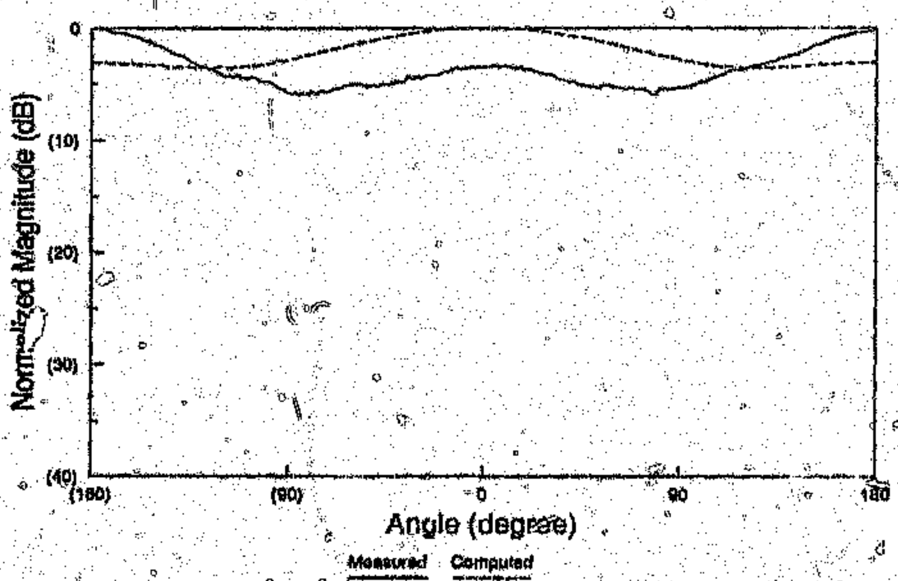

Figure 3.3 Pattern of middle antenna of model A with 1 antenna present at 1.0 GHz.

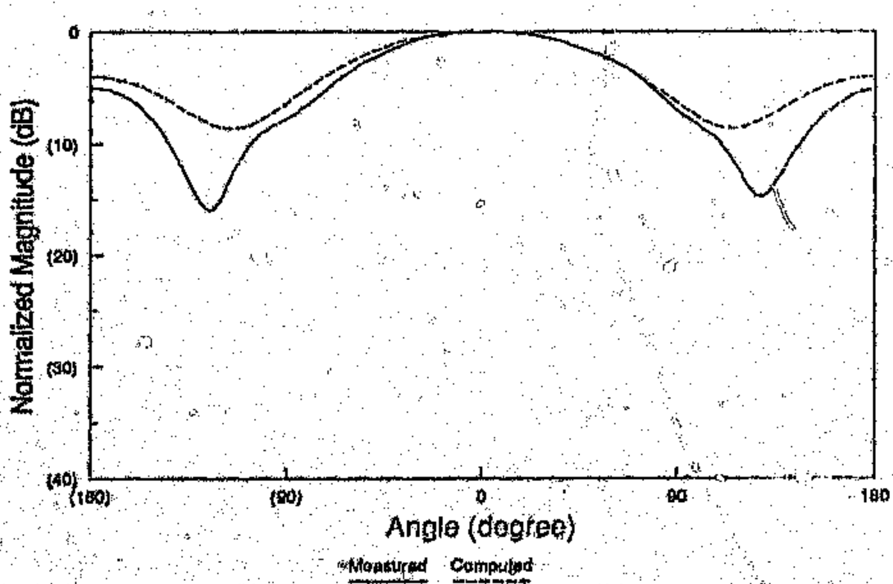

Figure 3.4 Pattern of middle antenna of model A with 1 antenna present at 2.0 GHz.

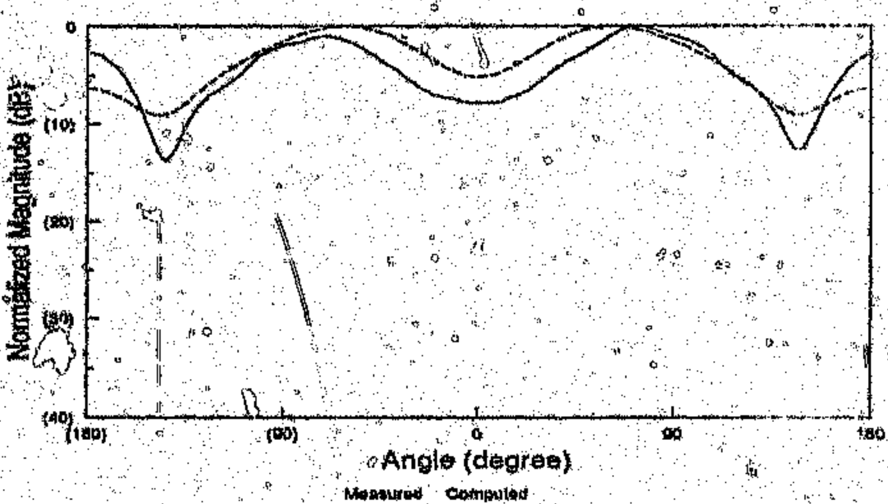

Figure 3.5 Pattern of middle antenna of model A with 1 antenna present at 3.0 GHz.

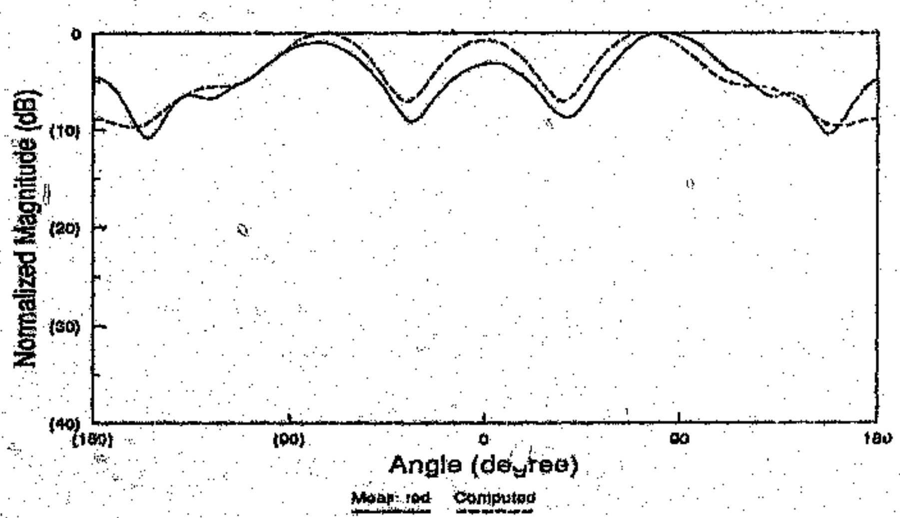

Figure 3.6 Pattern of middle antenna of model A with 1 antenna present at 4.0 GHz.

3.4 Second model. (Model B)

A drawing of the second model is shown in figure 3.7. This model includes all features of the first model. It further includes all vertical plates connected to the antenna platform. The model was discretised for a maximum frequency of 4.0 GHz. A total of 717 segments is used in this model for the ship, with 4 segments used for each antenna represented on the ship.

Figures 3.8 to 3.11 show the radiation pattern of the middle antenna of model B compared to the measured pattern. No other antenna is present.

As can be seen from the figures, the comparison of the pattern in the forward scattered area is relativ' jood, but the backward pattern is not as good, although it is better than the results obtained with the previous model.

Figures 3.12 and 3.13 show the magnitude of the currents flowing on the surface of the structure.

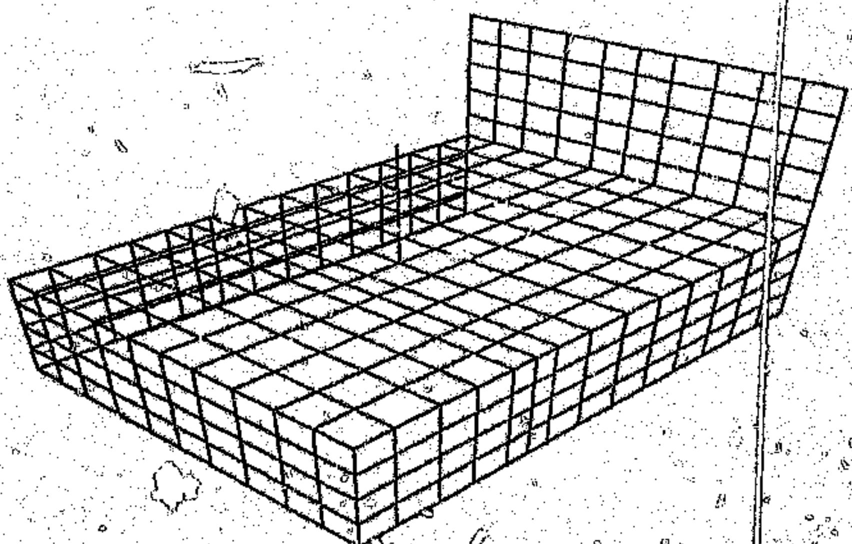

Figure 3.7 Discretised show of ship for model B.

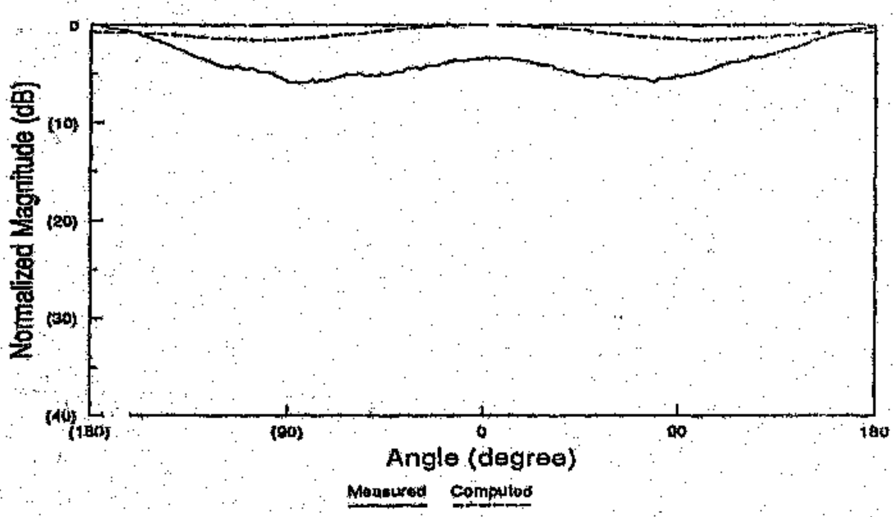

Figure 3.8 Pattern of middle antenna of model B with 1 antenna present at 1.0 GHz.

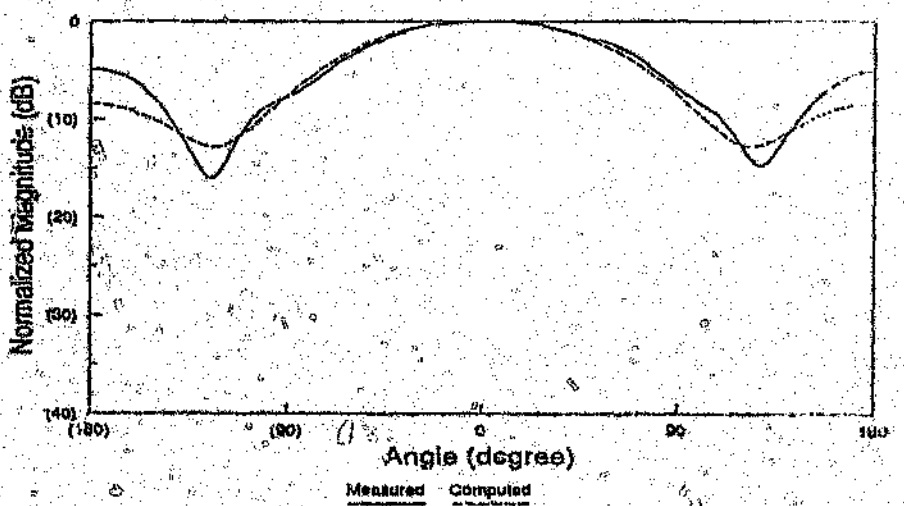

Figure 3.9 Pattern of middle antenna of model B with 1 antenna present at 2.0 GHz.

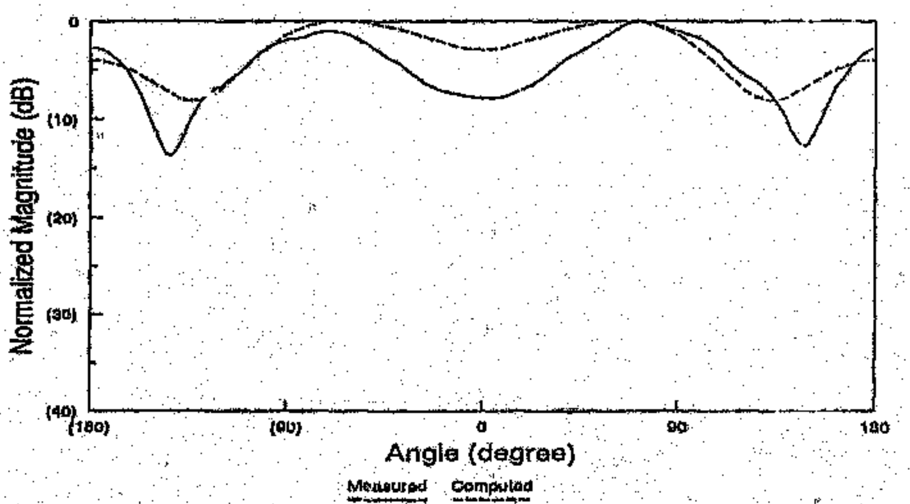

Figure 3.10 Pattern of middle antenna of model B with 1 antenna present at 3.0 GHz.

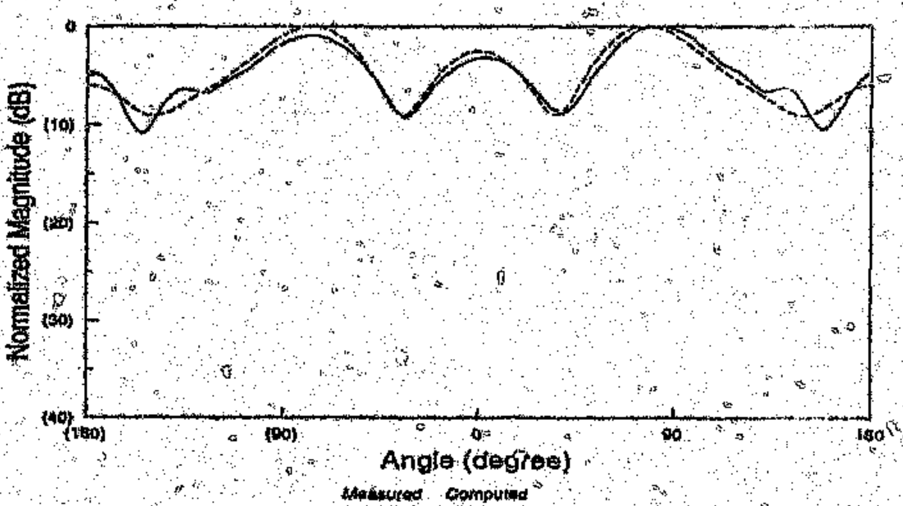

Figure 3.11 Pattern of middle antenna of model B with 1 antenna present at 4.0 GHz.

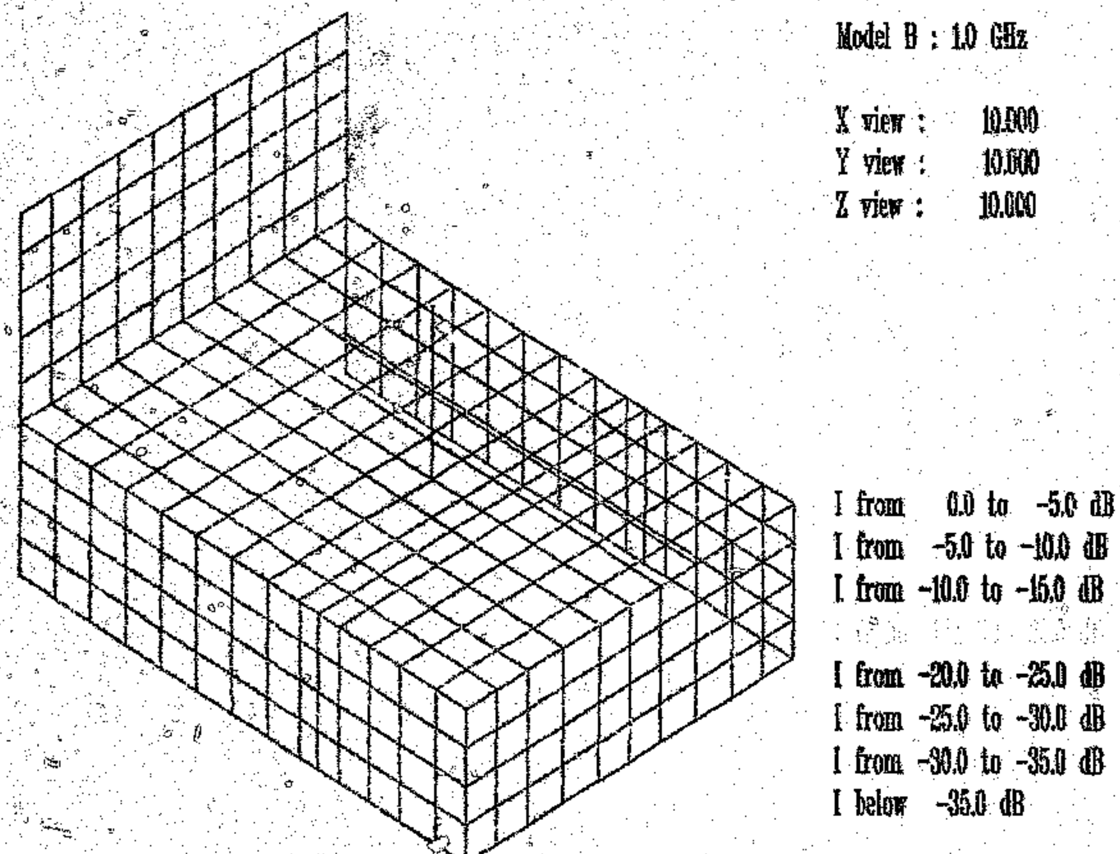

Figure 3.12 Current flow on model B for middle antenna active with 1 antenna present at 1.0 GHz (scale 5 dB/div).

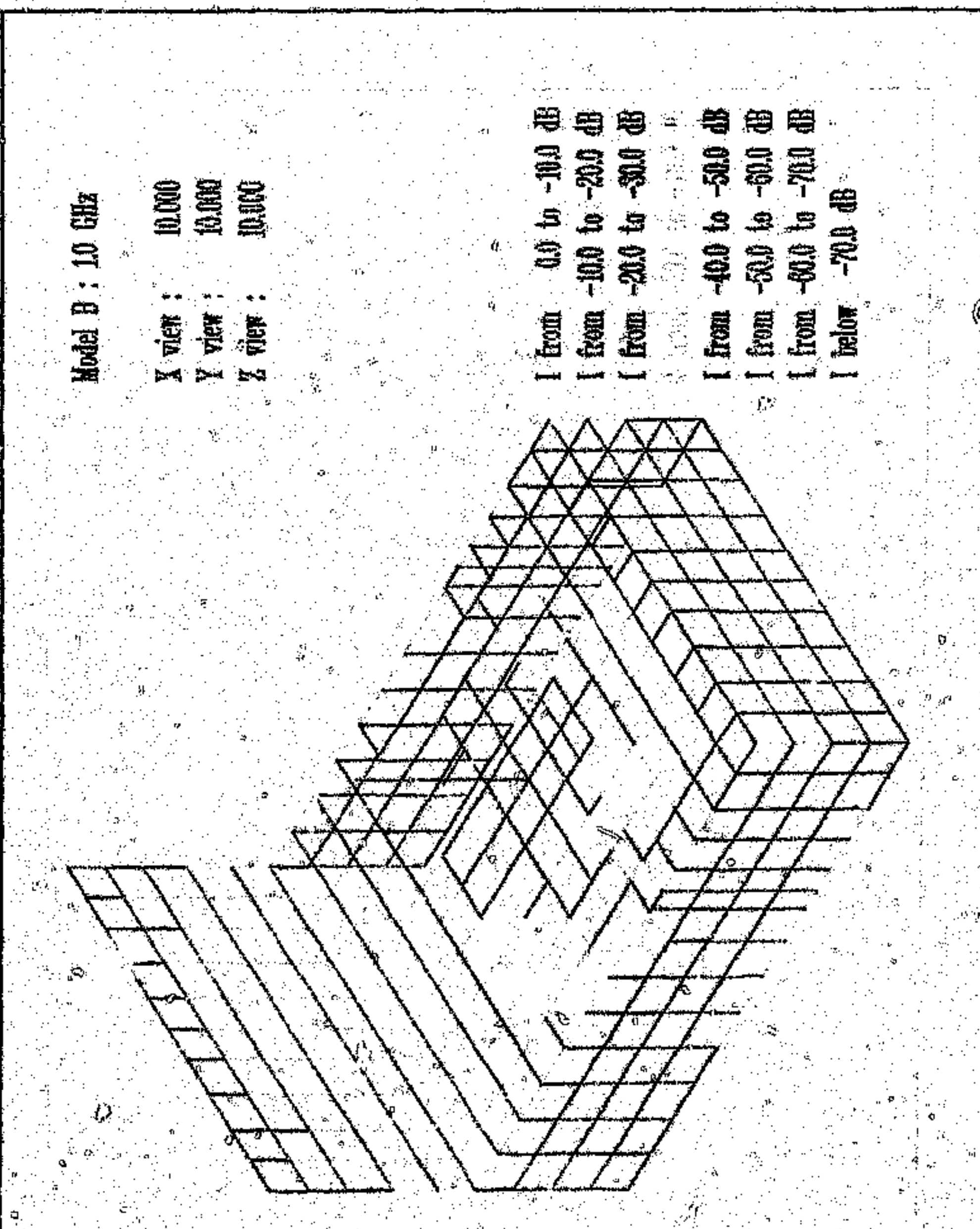

Figure 3.13 Current flow on model B for middle antenna active with 1 antenna present at 1.0 GHz (scale 10 dB/div).

3.5 Third model. (Model C)

A drawing of the third model is shown in figure 3.14. This model includes all features of the previous model (model B). A further addition is the highest deck including the vertical plates connected to it. The model was discretised for a maximum frequency of 4.0 GHz. A total of 1287 segments are used in this model for the ship, with 4 segments used for the antenna.

Figures 3.15 to 3.18 show the radiation pattern of the middle antenna of model C compared to the measured pattern with no other antenna present.

As can be seen from the figures, the comparison of the pattern in the forward scattered area is relative good, but the backward pattern is not as good. The results do not differ significant from those computed using model B.

Figures 3.19 and 3.20 show the magnitude of the currents flowing on the surface of the structure.

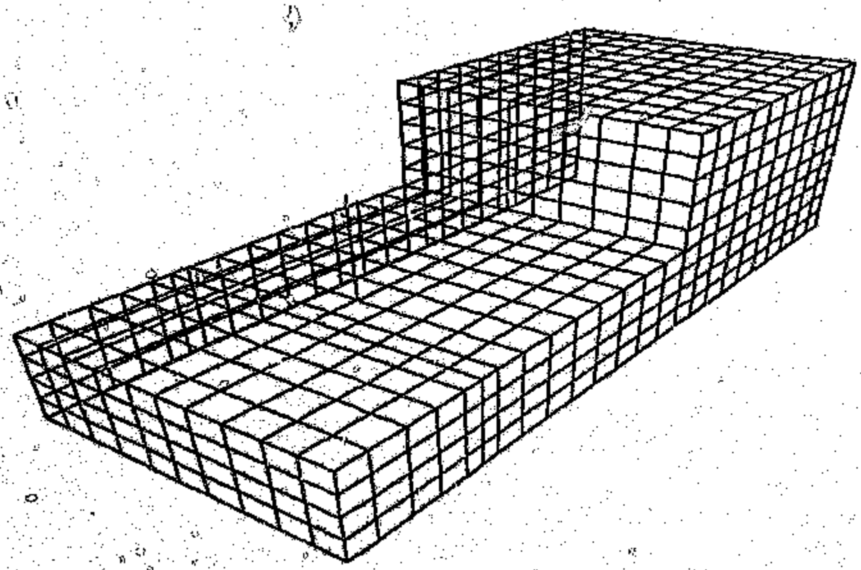

Figure 3.14 Discretised show of ship for model C.

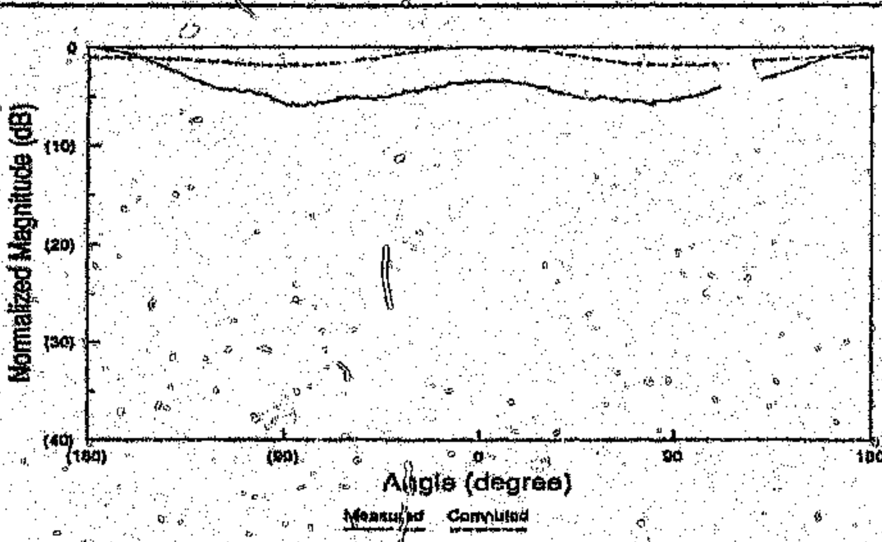

Figure 3.15 Pattern of middle antenna of model B with 1 antenna present at 1.0 GHz.

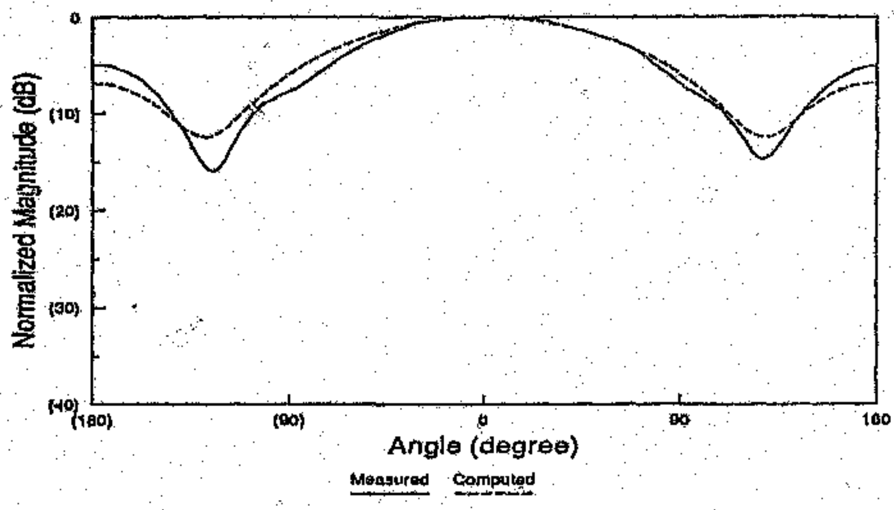

Figure 3.16 Pattern of middle antenna of model B with 1 antenna present at 2.0 GHz.

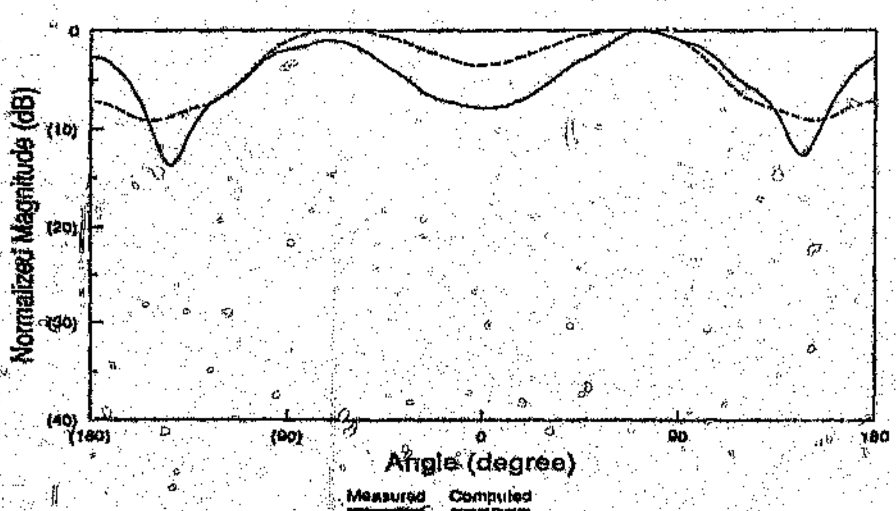

Figure 3.17 Pattern of middle antenna of model B with 1 antenna present at 3.0 GHz.

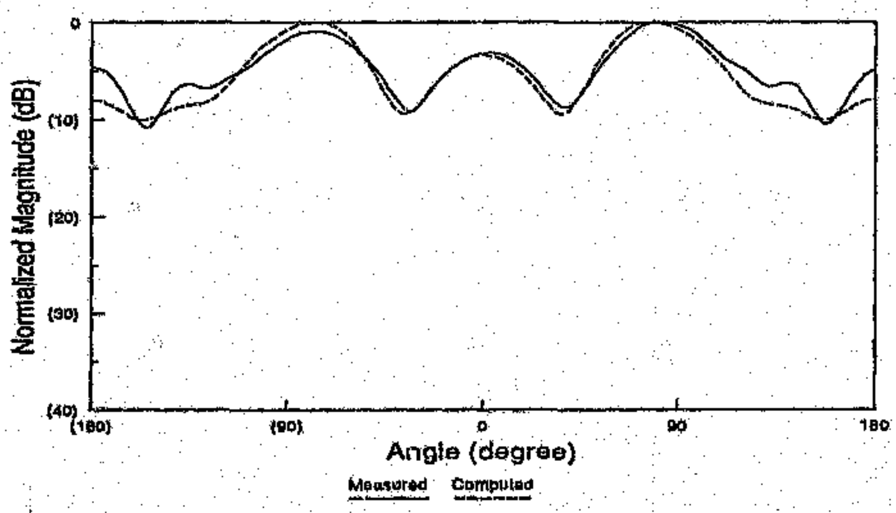

Figure 3.18 Pattern of middle antenna of model B with 1 antenna present at 4.0 GHz.

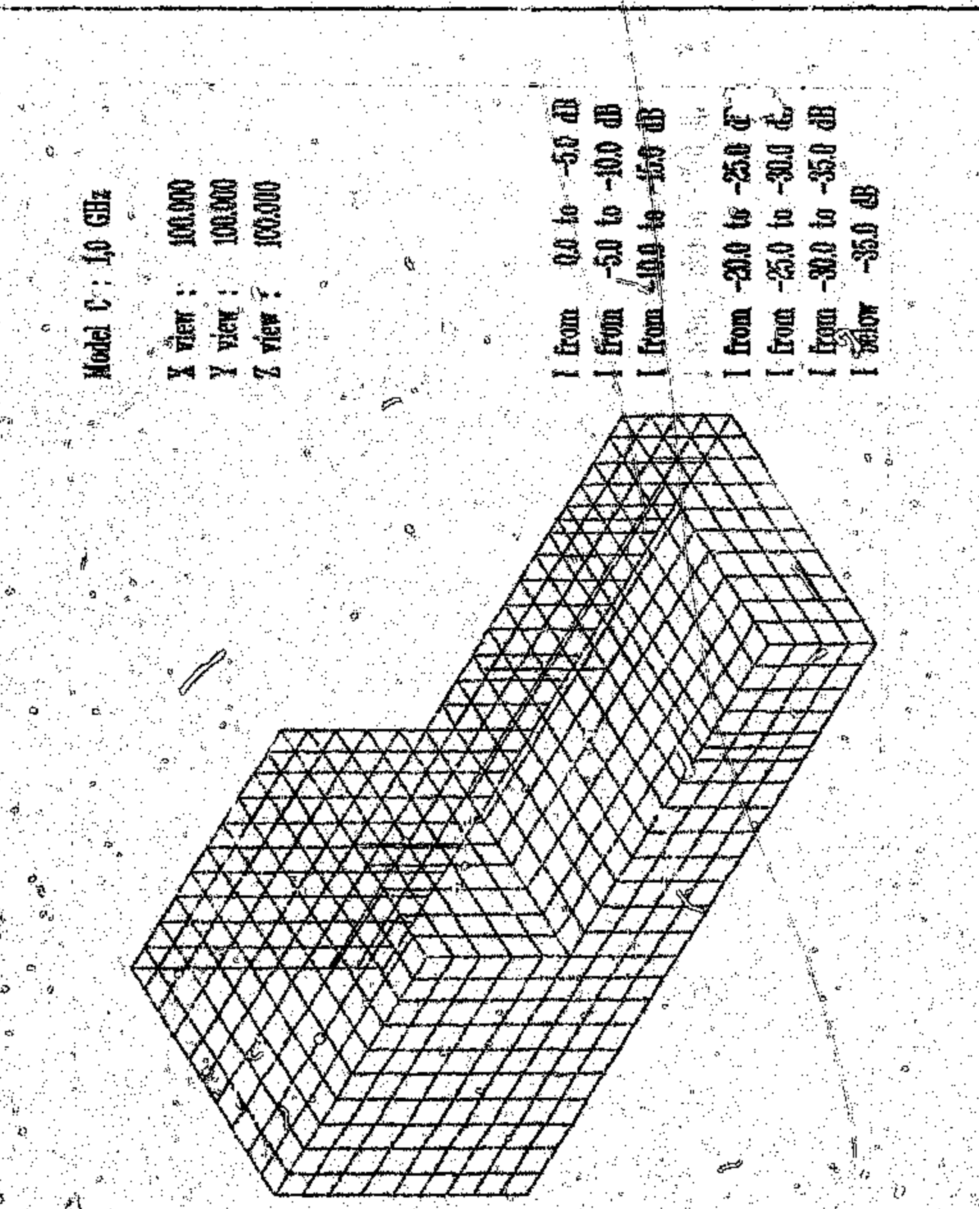

Figure 3.19 Current flow on model C for middle antenna active with 1 antenna present at 1.0 GHz (scale 5 dB/div).

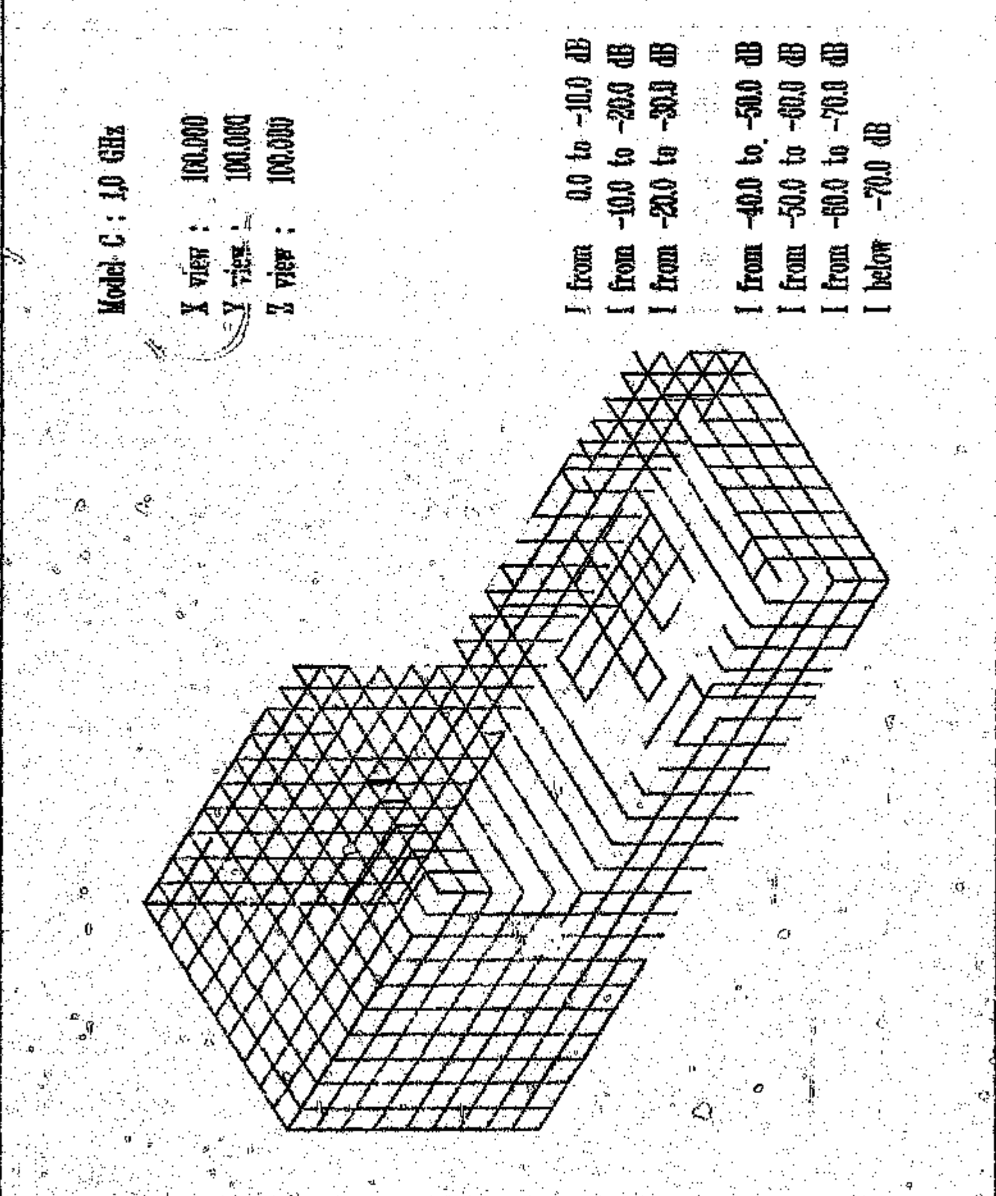

Figure 3.20 Current flow on model C for middle antenna active with 1 antenna present at 1.0 GHz (scale 10 dB/div).

3.6 Discussion

The comparison of the computed patterns using the different models is shown in figures 3.21 to 3.24. In these figures it can be seen that there are a very significant difference between the patterns of the first and second model, but a relative small difference between the patterns of the second and third model.

The observation can thus be made that the currents on the radiating platform flow around the sides of the top platform to the sides of the ship. The currents does not however flow in a substantial way onto the higher platform and the sides connected to it. From this it follows that only a relative small portion of the complete ship needs to be modelled to get reasonable results.

If one looks at the flow of current on the model (figures 3.12, 3.13, 3.19 and 3.20) it is possible to see that the currents are higher at the edges of plates than on regions next to edges. One would expect it to be this way if one thinks of the asymptotic (high frequency) solution which can be made in terms of edge currents [22]. Edge diffraction is also considered a local effect, so the currents must be local to the area where diffraction occurs [23].

Another observation that can be made is that the results are consistently better at the high frequency end (4 GHz) than at the low frequency end (1 GHz). As the mesh is electromagneticly coarser at higher frequencies, one would rather expect that the results must get worse as the frequency increase. The structure is also larger electromagneticly at higher frequencies, so that the simplifications made in ignoring substantial parts of the structure are far less significant.

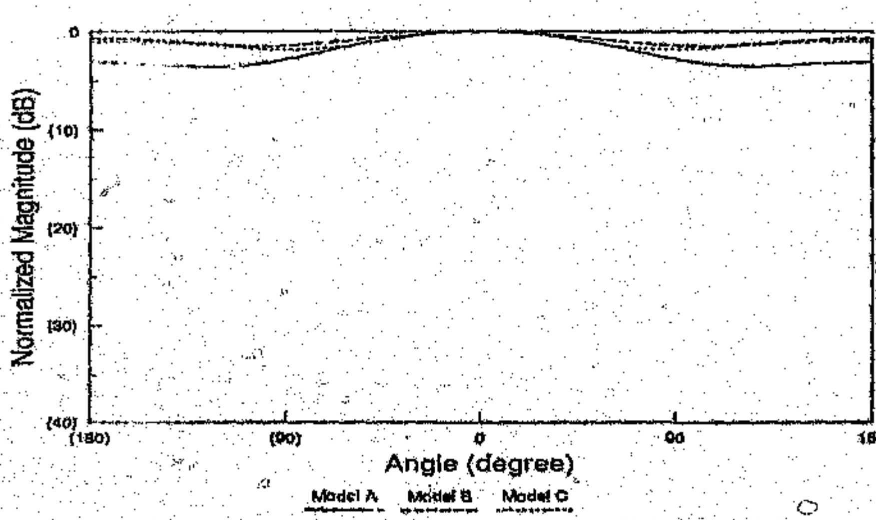

Figure 3.21 Comparison between the computed patterns of the antenna at 1 GHz using three models.

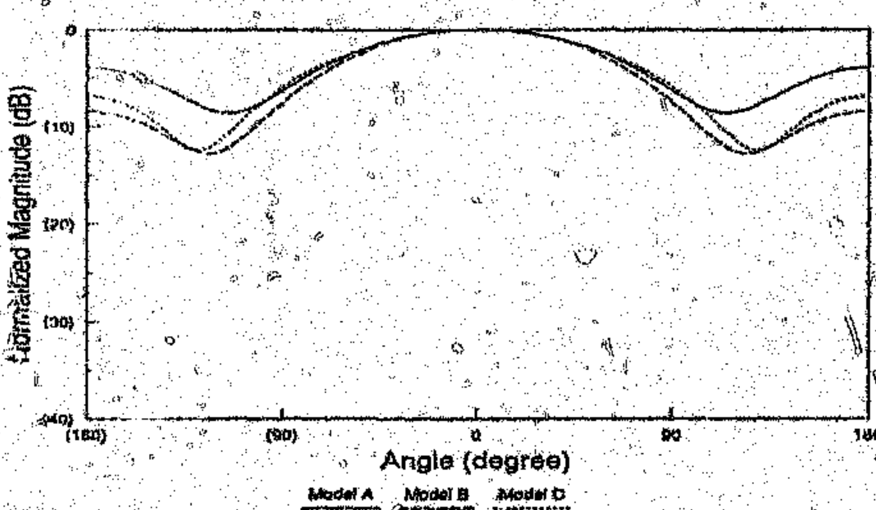

Figure 3.22 Comparison between the computed patterns of the antenna at 2 GHz using three models.

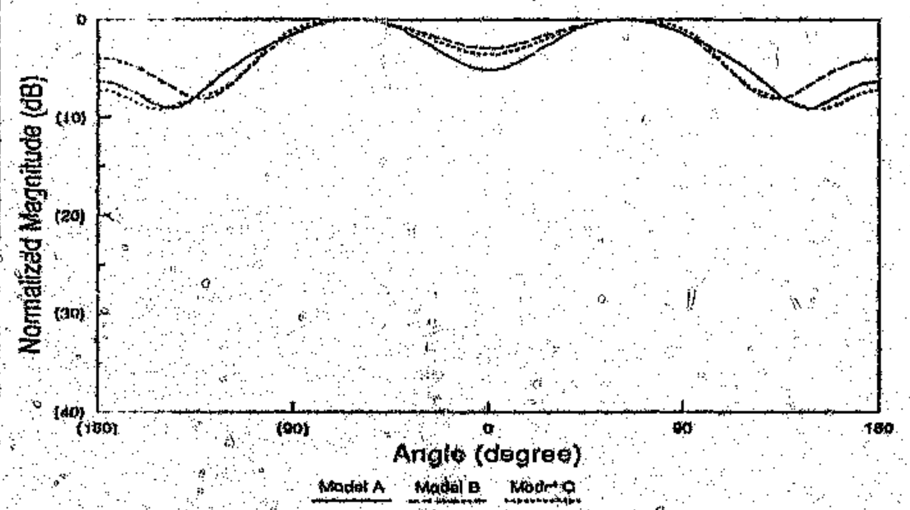

Figure 3.23 Comparison between the computed patterns of the antenna at 3 GHz using three models.

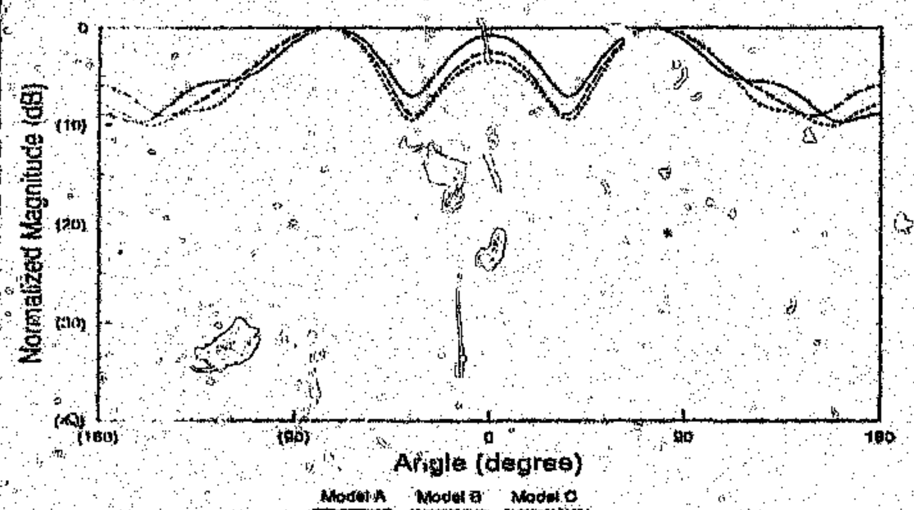

Figure 3.24 Comparison between the computed patterns of the antenna at 4 GHz using three models.

4 CONCLUSION

4.1 Summary

From the literature study done, it became clear that very little is published on how to model big structures such as ships. After investigating different modelling techniques, it was decided to further investigate the Method of Moments.

Different Method of Moments codes were investigated using a resonant dipole. The results of this investigation resulted in choosing the NEC2 computer program for further work.

Because of the need to model surfaces, and the unavailability of a reliable surface patch code, an investigation into wire grid modelling was launched. The following conclusions were reached:

* For a rectangular surface a square and triangular grid have similar performance for the same number of segments.

* Rectangular grids must have a spacing between wi es of not more than $\frac{1}{10}\lambda$.

* Triangular grids must have sides of not more than $\frac{1}{8}\lambda$.

* The wire radius must be such that the total wire surface must be equal to the total surface of the plate to modelled (twc times the surface of one side of the plate.

* The wire radius of a rectangular grid must be 0.159 times the length of the wire segments.

* The wire radius of a triangular grid must be 0.09 times the length of the wire segments.

An investigation into antennas on a simple ship was then launched. Three different computer (NEC2) models of increased complexity were built. Comparisons were made with measurements. The computed patterns were normally within 1 to 3 dB of the measured patterns.

No complete ship computer (NEC2) model could be built because of a limitation on computer memory and computational power. It is thus very difficult to determine if the few discrepancies between measured and predicted models are because parts of the ship were missing or some other reason. Because of the tremendous advances being made presently in computer technology, it is expected that a complete ship could be modelled in about five years.

4.2 Further work

4.2.1 Modelling of VHF and UHF antennas on masts on a ship

The Method of Moments can also be used to model VHF and UHF antennas on open masts on a ship. Open masts is meant to apply to masts that are built from metal in a lattice type manner, so that most of area of the mast is open. In this case the antennas are modelled with thin wires similar to the antennas (folded dipoles, resonant whips, etc.). The mast is modelled with wires of the correct diameter. The rest of the ship will be modelled by an infinite groundplane, or the mast is assumed to be in free space. Work on the modelling of VHF antennas on open masts has previously been done, although not for ships.

4.2.2 The use of the Geometrical Theory of Diffraction to calculate the patterns of UHF and microwave antennas mounted on masts on ships

The GTD can be used to calculate the pattern of UHF and microwave antennas mounted on closed masts on ships. Closed masts is meant to apply to masts that are built so as to present a closed area to the antenna, or where the dimensions of the structural members is such that they can be modelled by flat plates. In the case of closed masts, the mast is modelled by flat plates that represent the shape of the mast. The rest of the ship may be modelled by another set of plates with elliptic cylinders (for funnels) if so desired. The antenna is modelled by its pattern alone and the reflections and diffraction from the ship's structure are taken into account in calculating an new radiation pattern.

4.2.3 An deeper investigation into hybrid methods

The hybrid method appears to be able to solve a number of problems where one wants to work at a frequency where too many unknowns appear in a Method of

Moment solution and the GTD is not yet valid. Very little experience has been obtained yet in the application of this technique and it is felt that a thorough investigation of the method is called for.

4.2.4 The use of patches for the modelling of large surfaces

A few results of the use of patches for modelling large surfaces were calculated. These results do not compare well with measurements (and are thus not shown). It is felt that the reasons for the lack of accuracy in the results should be investigated. New models for patches to model surfaces have been found and should be investigated.

It is felt that if the problems in the patch formulation have been solved, it should give a much more reliable and accurate way of modelling large surfaces as the physical problem is solved correctly, and no unphysical current distribution is enforced on the surface.

5 REFERENCES

1. Stutzman, W. L. and Thiele, G. A., *Antenna Theory and Design*, New York: John Wiley and Sons, 1981.

2. Moore, J. and Pizer, R. (Ed), *Moment Methods in Electromagnetics*, Letchworth: Research Studies Press Ltd., 1984.

3. Butler, C. M. and Wilton, D. R., Analysis of various techniques applied to thin wire structures, *IEEE Transactions on Antennas and Propagation*, Vol. AP-23, July 1975, pp 534-540.

4. Pearson, '. W. and Butler, C. M., Inadequacies of collocation solutions to Pocklington-type models of thin-wire structures", *IEEE Transactions on Antennas and Propagation*, Vol. AP-23, March 1975, pp 295-298.

5. Richmond, J. H., A wire grid model for scattering by conducting bodies, *IEEE Transactions on Antennas and Propagation*, Vol. AP-14, November 1966, pp 782-786.

6. Calmon, L. C. and Smith, M. S., Prediction and measurement of near fields for antennas on structures, *Journal of the Institution of Electronic and Radio Engineers*, Vol 55, No 11/12, November/December 1985, pp 407-414.

7. Jambrina, J. L. F. and Andrés, F. L., Analysis of shipboard HF antennas with the PDMPH2 computer code, *4'th International Conference on HF Radio Techniques*, IEE London, Conference Publication no 284, 11-14'th April 1988.

8. Kubina, S. J. and Larose, C., A NEC topside antenna case study with DIDEC and SPECTRUM: Model generation and current display codes, Source unknown.

9. Woodman, K. F. and Stemp, B. E., Shipborne Antenna Modeling, *Microwave Journal*, April 1979, p73.

10. Newman, E. H., Alexandropoulos, P. and Walton, E. K., Polygonal plate modelling of realistic structures, *IEEE Transactions on Antennas and Propagation*, Vol. AP-32, No. 7, July 1984, pp 742-747.

11. Rockway, J. W. and Du Brul, D. W., Performance prediction analysis for shipboard antenna systems, *Naval Engineers Journal*, Vol. 89, No. 5, October 1977, pp 33-40.

12. Woodman, K. F. and Stemp, B. E., Shipborne antenna modelling, *Microwave Journal*, April 1979, pp 73-81.

13. Chuang, C. W. and Burnside, W. D., A diffraction coefficient for a cylindrical truncated planar surface, *IEEE Transactions on Antennas and Propagation*, Vol. AP-28, No. 2, March 1980, pp 177-182.

14. Burke, G. J. and Pogio, A. J., *Numeric Electromagnetics Code (NEC) - Method of Moments - Volume I, Part I: Program Description - Theory*, Naval Ocean Systems Center, TD116, January 1981.

15. Burke, G. J. and Pogio, A. J., *Numeric Electromagnetics Code (NEC) - Method of Moments - Volume 1, Part II: Program Description - Code*, Naval Ocean Systems Center, TD116, January 1981.

16. Burke, G. J. and Pogio, A. J., *Numeric Electromagnetics Code (NEC) - Method of Moments - Volume 2, Part III: User's Guide*, Naval Ocean Systems Center, TD116, January 1981.

17. Richmond, J. H., *Radiation and Scattering by Thin-wire Structures in the Complex Frequency Domain*, Ohio State University ElectroScience Laboratory interaction note 202, May 1974.

18. Richmond, J. H., *Computer Program for Thin-Wire Structures in a Homogeneous Nonducting Medium*, Ohio State University ElectroScience Laboratory Interaction Note 203, June 1974.

19. Newman, E. H. and Pozar, D. M., Electromagnetic modelling of composite wire and surface geometries, *IEEE Transactions on Antennas and Propagation*, Vol. AP-26, November 1978, pp 784-789.

20. Schelkunoff, S. A., On diffraction and radiation of electromagnetic wave, *Physical Review*, Vol. 56, 15 August 1939, p 308.

21. Rumsey, V. H., Reaction concept in electromagnetic theory, *Physical Review*, Vol. 94, 15 June 1954, pp 1483-1491.

22 Ryan, C. E. and Peters, L., Evaluation of edge-diffracted fields including equivalent currents for the caustic regions, *IEEE Transactions on Antennas and Propagation*, Vol. AP-17, No. 3, May 1969, pp 292-299.

23 Kouyoumjian, R. G. and Pathak, P. H., A Uniform Geometrical Theory of Diffraction for a edge in a perfectly conducting surface, *Proceedings of the IEEE*, Vol. 62, No. 11, November 1974, pp 1448-1461.

24 Law, Preston E., *Shipboard Electromagnetics*, Norward, MA : Artech House, 1987.

25 Ludwig, Arthur C., Wire grid modeling of surfaces, *IEEE Transactions on Antennas and Propagation*, Vol. AP-35, No. 9, September 1987, pp 1045-1048.

APPENDIX A. INTEGRAL EQUATIONS

The following is a derivation of the most important integral equations used in this work. This derivation is based on [2] pp 17-27.

A.1 Maxwell's Equations

We start with Maxwell's equations (assuming a homogenous medium and a $e^{j\omega t}$ time dependance)

$$\overline{\nabla} \times \overline{E} = -j\omega\mu\overline{H} \tag{A.1}$$

$$\overline{\nabla} \cdot \overline{E} = \rho/\varepsilon \tag{A.2}$$

$$\overline{\nabla} \times \overline{H} = j\omega\varepsilon\overline{E} + \overline{J} \tag{A.3}$$

$$\overline{\nabla} \cdot \overline{H} = 0 \tag{A.4}$$

Equation (A.4) requires that $\overline{H}$ be expressible as the curl of a vector field.

$$\overline{H} = \frac{1}{\mu}\overline{\nabla} \times \overline{A} \tag{A.5}$$

where $\overline{A}$ is the magnetic vector potential.

Equation (A.1) now gives

$$\overline{E} = -j\omega\overline{A} - \overline{\nabla}\phi \tag{A.6}$$

where ϕ is the electric scalar potential.

The Helmholtz equations are now obtained:

$$\nabla^2\overline{A} + k^2\overline{A} = -\mu\overline{J} \tag{A.7}$$

$$\nabla^2\phi + k^2\phi = -\rho\varepsilon \tag{A.8}$$

where $k^2 = \omega^2\varepsilon\mu$ and k is called the propagation constant. The Lorentz' condition has now been imposed on ϕ:

$$\overline{\nabla} \cdot \overline{A} = -j\omega\varepsilon\mu\phi \tag{A.9}$$

For good conductors (Where the current $\overline{J}$ and charge ρ reside on or very close to the surface) Helmholtz's equations can be solved:

$$\overline{A}(\overline{r}) = \mu \int\int_s \overline{J}_s(r')\frac{e^{-jkR}}{4\pi R}dS' \tag{A.10}$$

and

$$\phi(\overline{r}) = \frac{1}{\varepsilon}\int\int_s \rho_s(r')\frac{e^{-jkR}}{4\pi R}dS' \tag{A.11}$$

where integration is over the whole surface, S, of the body, $R = |\overline{r} - \overline{r}'|$ is the distance between the observation point $\overline{r}$ (outside the surface of the conductor) and some point $\overline{r}'$ on the surface of the conductor, $\overline{J}_s$ and ρ_s are surface current and charge den**ies and μ and ε are permeability and permittivity for the medium outside the conductor.

The law of conservation of charge also applies and this can be expressed as

$$\overline{\nabla} \cdot \overline{J} = -j\omega\rho \tag{A.12}$$

or

$$\overline{\nabla}_s \cdot \overline{J}_s = -j\omega\rho_s \tag{A.13}$$

where $\overline{\nabla}_s$ denotes surface divergence.

The following boundary conditions apply between two different materials:

$$(\overline{E}^{(1)} - \overline{E}^{(2)}) \times \hat{n} = \overline{0} \tag{A.14}$$

$$\hat{n} \cdot (\overline{D}^{(1)} - \overline{D}^{(2)}) = \rho_s \tag{A.15}$$

$$\hat{n} \times (\overline{H}^{(1)} - \overline{H}^{(2)}) = \overline{J}_s \tag{A.16}$$

$$\hat{n} \cdot (\overline{B}^{(1)} - \overline{B}^{(2)}) = 0 \tag{A.17}$$

where the superscript (1) and (2) refer to the field on either side of the boundary and $\hat{n}$ is the unit normalvector to the surface pointing into region (1).

A.2 The potential Integro-Differential Equation

The potential integro-differential equation is now given for a thin-wire.

If the wires are thin compared to the wavelength and the distance between wire junctions is sufficiently long compared to the radius, the following assumptions are valid:

(i) Current flow is parallel to the axis.

(ii) The axially-directed surface current density is uniformly distributed around the circumference.

(iii) The circumferential component of the electric surface current is negligible.

(iv) Axial electric surface current can be replaced by a line current $\overline{I}$ flowing along the wire axis:

$$\overline{I} = 2\pi a \overline{J}_s \tag{A.18}$$

(v) Axial surface charge can be replaced by a line charge q per unit length distributed along the wire axis:

$$q = 2\pi a \rho_s \tag{A.19}$$

Equations (A.10), (A.11) and (A.13) can now be simplified to:

$$\overline{A}(\overline{r}) = \mu \int_{wire} \overline{I}(l') \frac{e^{-jkR}}{4\pi R} dl' \tag{A.20}$$

$$\phi(\bar{r})=\frac{1}{\varepsilon}\int_{wire}q(l')\frac{e^{-jkR}}{4\pi R}dl' \tag{A.21}$$

$$q(l)=\frac{j}{\omega}\frac{d}{dl}I(l) \tag{A.22}$$

where l is the measure of length along the wire.

The only boundary condition to be satisfied is the one concerning the axial component of the electric field and this is from equation (A.14):

$$\hat{l}\cdot(\overline{E}^{(1)}-\overline{E}^{(2)})=0 \tag{A.23}$$

where $\hat{l}$ is a unit vector parallel to the wire.

If we now assume that the body will be illuminated by a plane wave of known amplitude and polarisation, the total electric field may be written as:

$$\overline{E}=\overline{E}^{i}+\overline{E}^{s} \tag{A.24}$$

with $\overline{E}^{i}$ the known incident electric field and $\overline{E}^{s}$ the unknown electric filed scattered from the body.

Taking equations (A.6), (A.20) and (A.21) into account the following equations follow:

$$\overline{E}^{s}=-j\omega\overline{A}^{s}-\overline{\nabla}\phi^{s} \tag{A.25}$$

$$\overline{A}^s(\bar{r}) = \mu \int_{wire} I(l') \frac{e^{-jkR}}{4\pi R} dl' \qquad (A.26)$$

$$\overline{\phi}^s(\bar{r}) = \frac{1}{\varepsilon} \int_{wire} q(l') \frac{e^{-jkR}}{4\pi R} dl' \qquad (A.27)$$

with the boundary condition (from equation (A.23))

$$\hat{l} \cdot (\overline{E}^i + \overline{E}^s + \overline{E}^{(2)}) = 0 \qquad (A.28)$$

For a perfect conducting material $\overline{E}^{(2)} = 0$ while for a wire of finite conductivety it may be calculated (*(2)* Chapter 12) approximately as

$$\overline{E}^{(2)} = Z_\omega \overline{J} \qquad (A.29)$$

where Z_ω is the known impedance per unit length of the wires.

By substituting equations (A.22), (A.25), (A.27) and (A.29) in equation (A.28) the potential integro-differential equation is obtained for the current:

$$Z_\omega I(l) - \hat{l} \cdot \overline{E}^i(l) = -j \int_{wires} \left(\omega\mu\, \hat{l} \cdot \vec{I}(l) + \frac{1}{\omega\varepsilon} \frac{dI(l')}{dl'} \frac{\partial}{\partial l} \right) \frac{e^{-jkR}}{4\pi R} dl' \qquad (A.30)$$

A.3 Pocklington's Integral Equation

To get Pocklington's integral equation one substitutes equation (A.9) into equation (A.6) to give:

$$j\omega\varepsilon\overline{E} = \frac{1}{\mu}\left(k^2\overline{A} + \overline{\nabla}(\overline{\nabla} \cdot \overline{A})\right) \tag{A.31}$$

By going through the same procedure of expressing this equation in terms of currents, and taking the thin wire approximation one arrives at Pocklington's integral equation:

$$j\omega\varepsilon\left(Z_w I(l) - \hat{l} \cdot \overline{E}^i(\overline{r})\right) = \int_{wires} I(l')\left(-\frac{\partial}{\partial l}\frac{\partial}{\partial l'} + k^2\hat{l} \cdot \hat{l}'\right)\frac{e^{-jkR}}{4\pi R}dl' \tag{A.32}$$

where $\hat{l}$, $\hat{l}'$ are unit vectors lying along the wire at the observation point $\overline{r}$ and source point $\overline{r}'$ respectively.

A.4 The Reaction Integral Equation (RIE)

Consider a geometry of arbitrary shaped scatterers in a homogeneous medium as shown in figure A.1. S is the surface enclosing the scatterers and $\hat{n}$ is the unit outward normal to S. Note that S may be any closed surface such as solid surfaces, wires and combinations. The $e^{j\omega t}$ is suppressed. The sources $(\overline{J}_i, \overline{M}_i)$ generate the fields $(\overline{E}_i, \overline{H}_i)$ in free space and the field $(\overline{E}, \overline{H})$ in the presence of the scatterers. From Schelkunoff's surface-equivalence theorem [20] the field interior to the surface S (that is in the conducting medium) will vanish without changing the exterior fields if the surface current densities:

$$\overline{J}_s = \hat{n} \times \overline{H} \tag{A.33}$$

and

$$\overline{M}_s = \overline{E} \times \hat{n} \tag{A.34}$$

are introduced on the surface S (see figure A.2). The scattering obstacles may now be replaced by the ambient medium without altering the field anywhere external to the surfaces. The scattered field, radiated by $(\overline{J}_s, \overline{M}_s)$ in the ambient medium, is defined as (see figure A.3):

$$\overline{E}_s = \overline{E} - \overline{E}_i \tag{A.35}$$

$$\overline{H}_s = \overline{H} - \overline{H}_i \tag{A.36}$$

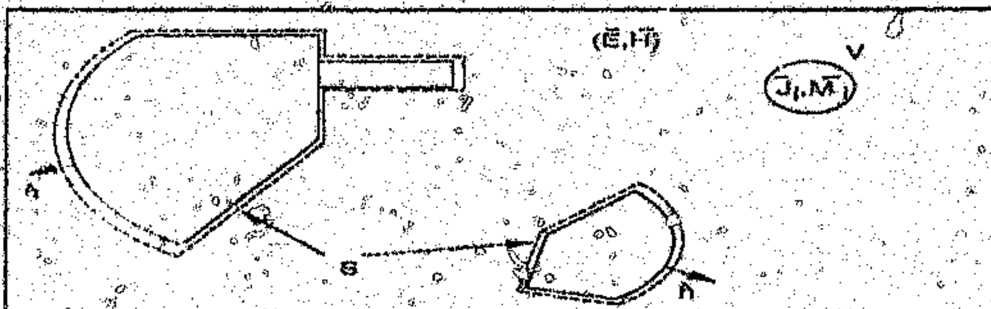

Figure A.1 The source $(\overline{J}_i, \overline{M}_i)$ generates the fields $(\overline{E}, \overline{H})$ in the presence of the scatterers.

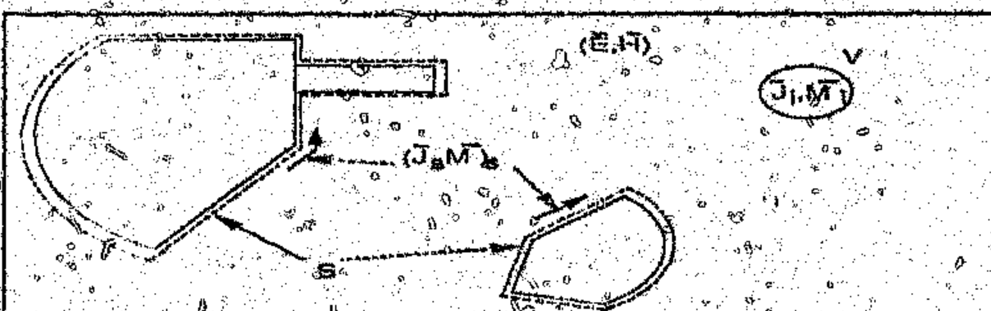

Figure A.2 Surface currents $(\overline{J}_s, \overline{M}_s)$ are placed on S without changing the exterior fields, but making field interior to S vanish.

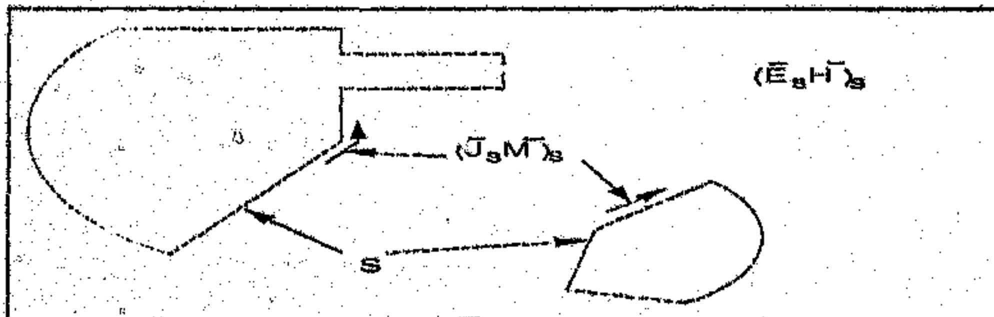

Figure A.3 Scattered field generated by $(\overline{J}_s, \overline{M}_s)$.

Since the interior of S has a null field, a test source $(\overline{J}_m, \overline{M}_m)$ enclosed by S, generating the fields $(\overline{E}_m, \overline{H}_m)$ in the ambient medium, will have zero reaction with the total field $(\overline{E}, \overline{H})$ thus:

$$\int\int_S (\overline{J}_m \cdot \overline{E}_s - \overline{M}_m \cdot \overline{H}_s)dS + \int\int_S (\overline{J}_m \cdot \overline{E}_i - \overline{M}_m \cdot \overline{H}_i)dS = 0 \qquad (A.37)$$

Using the reciprocity theorem yields

$$\int\int_S (\overline{J}_s \cdot \overline{E}_m - \overline{M}_s \cdot \overline{H}_m)dS + \int\int\int_V (\overline{J}_i \cdot \overline{E}_m - \overline{M}_i \cdot \overline{H}_m)dV = 0 \qquad (A.38)$$

where the volume integral is over the source $(\overline{J}_i, \overline{M}_i)$ volume.

Equation (A.38) is known as the Reaction Integral Equation (RIE) and was developed by Rumsey [21]. If electric current test sources are used, equation (A.38) reduces to the Electrical Field Integral Equation (EFIE) while the use of magnetic current test sources leads to the Magnetic Field Integral Equation (MFIE).

For conductors of finite conductivity the impedance boundary condition

$$\overline{M}_s = Z_s \overline{J}_s \times \hat{n} \tag{A.39}$$

is used. For perfect conductivity $Z_s = \overline{M}_s = 0$.

APPENDIX B. MEASUREMENTS ON SHIP MODEL

To verify the results obtained with the different numerical methods used, reliable results of a known case were needed. Because of the difficulty in obtaining such reliable results in the literature, measurements were made on a tin model as described in the text.

This measurements were made using the experimental setup as described in figure B.1. The main subsystems of this setup are the HP8510 Network Analyzer system used as the RF instrumentation, and the positioner system used for controlling the mechanical movement of the model. The whole system were placed under computer control so that the results could be obtained in computer readable form.

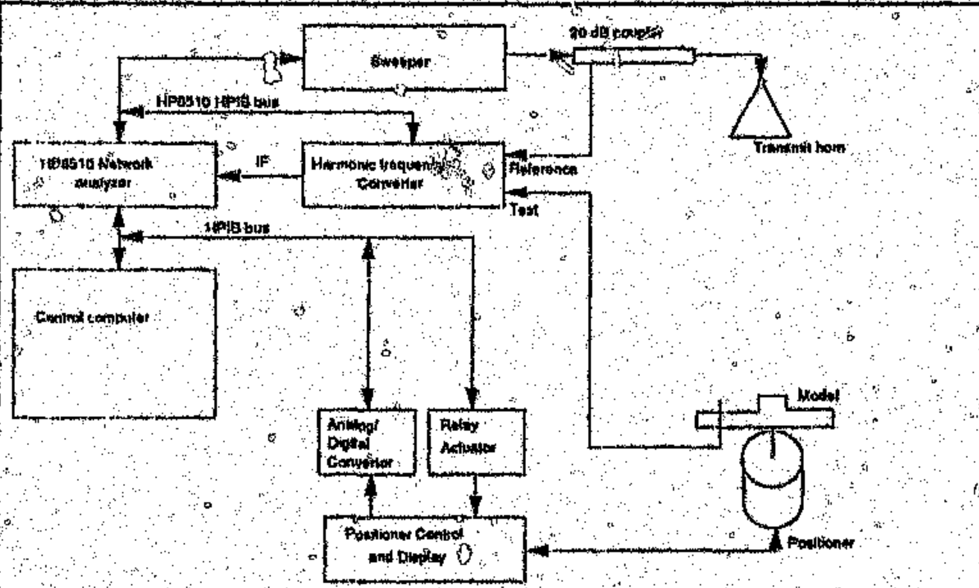

Figure B.1 Pattern measurement setup.

Figures B.2 to B.5 give patterns measured at frequencies between 1.0 and 4.0 GHz. Each plot gives the pattern measured at a range of 1m and at a range of 2m. As can be seen the two patterns are the same at all frequencies except at 1.0 GHz. At this frequency the one meter range is too small for the measurements. This is not due to the far field condition, but to the radiation pattern of the source horn at this frequency. In the text all comparisons to measured results are made with the 2m range data.

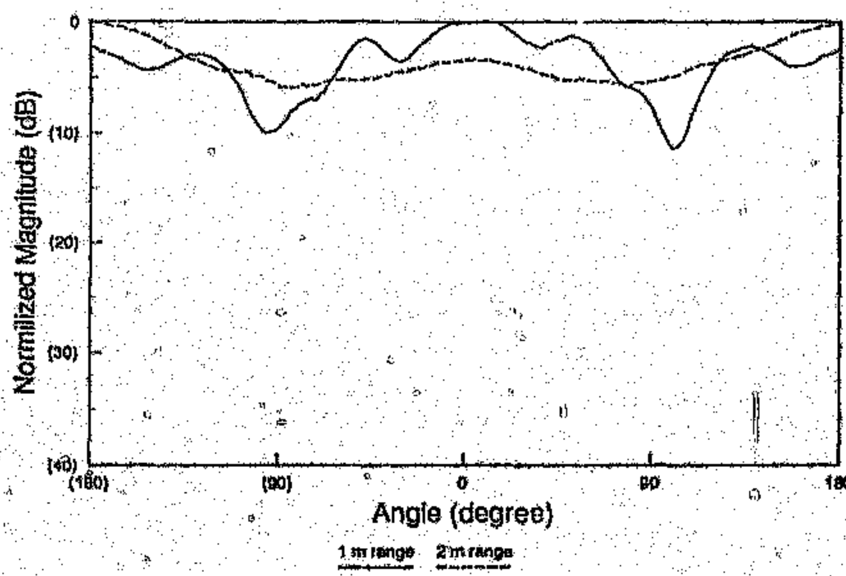

Figure B.2 Measured pattern of ship at 1.0 GHz at a range of 1.0 and 2.0 m.

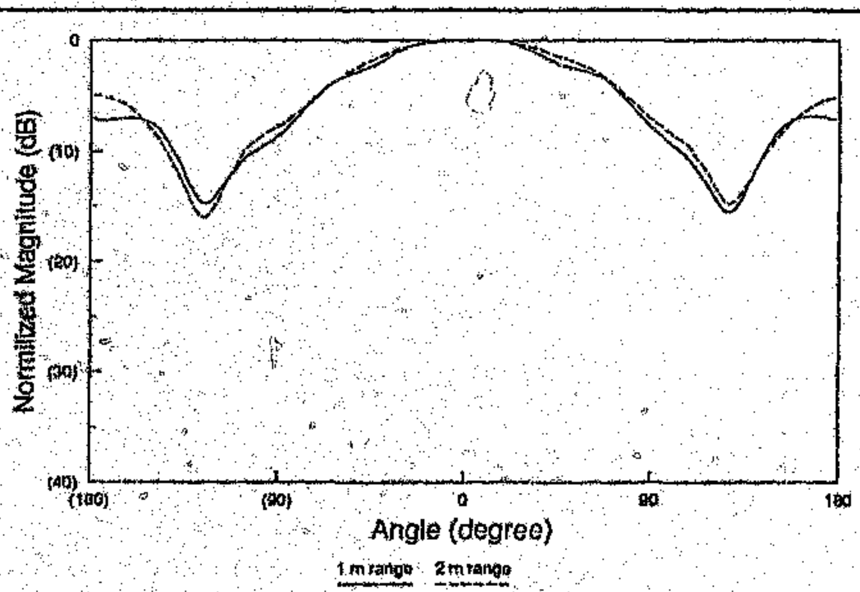

Figure B.3 Measured pattern of ship at 2.0 GHz at a range of 1.0 and 2.0 m.

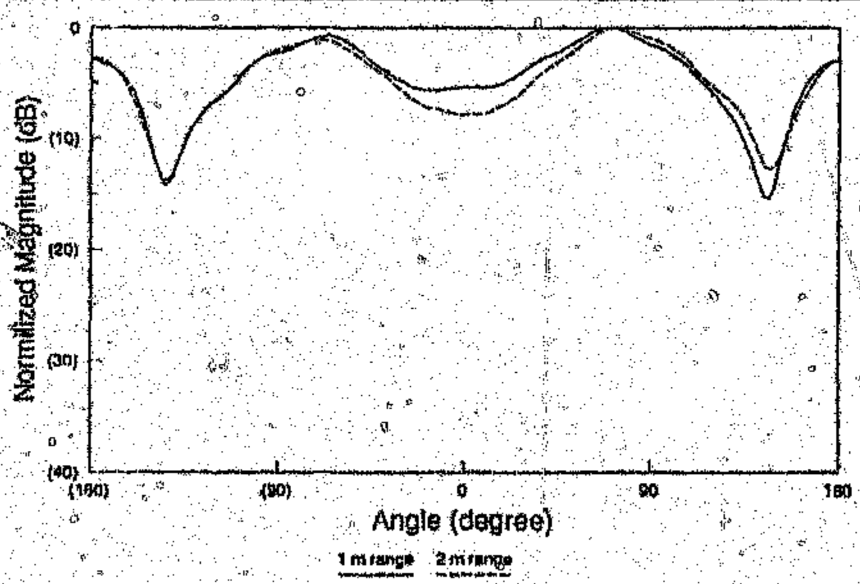

Figure B.4 Measured pattern of ship at 3.0 GHz at a range of 1.0 and 2.0 m.

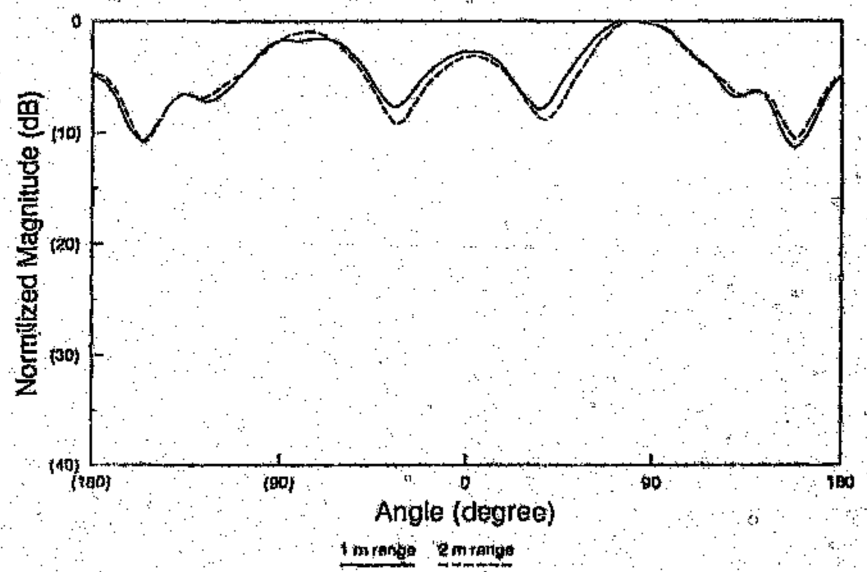

Figure B.5 Measured pattern of ship at 4.0 GHz at a range of 1.0 and 2.0 m.

APPENDIX C. TABULATED RESULTS OF DIPOLE STUDY

Table 2.1 Results obtained of dipole using NEC2.

Freq	3 segments		5 segments		7 segments		11 segments	
	Real	Imag	Real	Imag	Real	Imag	Real	Imag
290.	76.36	17.87	76.75	20.09	77.30	21.00	78.07	21.92
292.	77.60	23.48	78.19	25.59	78.85	26.48	79.75	27,38
294.	78.85	29.06	79.65	31.06	80.43	31.93	81.47	32.83
296.	80.12	34.60	81.14	36.52	82.05	37.38	83.22	38.28
298.	81.40	40.12	82.65	41.96	83.69	42.81	85.01	43.73
300.	82.70	45.61	84.18	47.38	85.36	48.24	86.83	49.17
302.	84.02	51.08	85.75	52.79	87.06	53.65	88.70	54.60
304.	85.34	56.51	87.33	58.18	88.79	59.06	90.60	60.03
306.	86.69	61.92	88.94	63.56	90.56	64.45	92.55	65.47
308.	88.05	67.31	90.58	68.93	92.36	69.84	94.54	70.90
310.	89.42	72.77	92.25	74.28	94.20	75.22	96.57	76.33

Table 2.2 Results obtained of dipole using THWIRE.

Freq	2 segments		4 segments		8 segments	
	Real	Imag	Real	Imag	Real	Imag
290.	66.36	14.86	74.19	13.77	76.52	15.40
292.	67.68	20.34	75.91	19.22	78.37	20.81
294.	69.03	25.82	77.67	24.66	80.27	26.22
296.	70.40	31.31	79.47	30.12	82.22	31.64
298.	71.80	36.82	81.31	35.58	84.21	37.06
300.	73.23	42.34	83.20	41.05	86.26	42.49
302.	74.68	47.87	85.13	46.52	88.36	47.93
304.	76.16	53.41	87.11	52.01	90.52	53.39
306.	77.67	58.98	89.14	57.51	92.73	58.85
308.	79.21	64.56	91.22	63.0[illegible]	95.00	64.32
310.	80.78	70.16	93.35	68.55	97.32	69.81

APPENDIX D. WIRE RADIUS OF A SQUARE GRID

Consider the geometry as shown in figure D.1 where a square plate of length a is considered. The segment length is l and the wire radius is r.

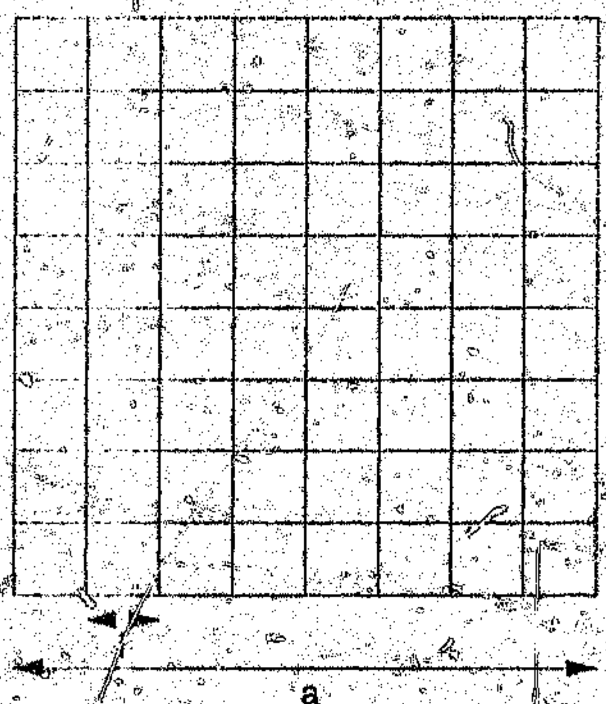

Figure D.1 Geometry of a square grid.

The surface of the square plate is a^2.

There are a total of $\frac{a}{l}$ segments on each wire. In each direction there are $\frac{a}{l}$ wires, thus a total of $2\frac{a}{l}\cdot\frac{a}{l}$ segments on the plate.

The area of a segment is $2\pi r l$.

As the total are of the wires must be equal to two times the area of the plate:

$$2\pi r l \cdot 2\frac{a}{l} \cdot \frac{a}{l} = 2a^2$$

or

$$r = \frac{1}{2\pi} l \approx 0.159 l$$

APPENDIX E. WIRE RADIUS OF A TRIANGULAR GRID

Consider the geometry as shown in figure E.1 where a triangular plate with all sides equal to a is considered. The segment length is l and the wire radius is r.

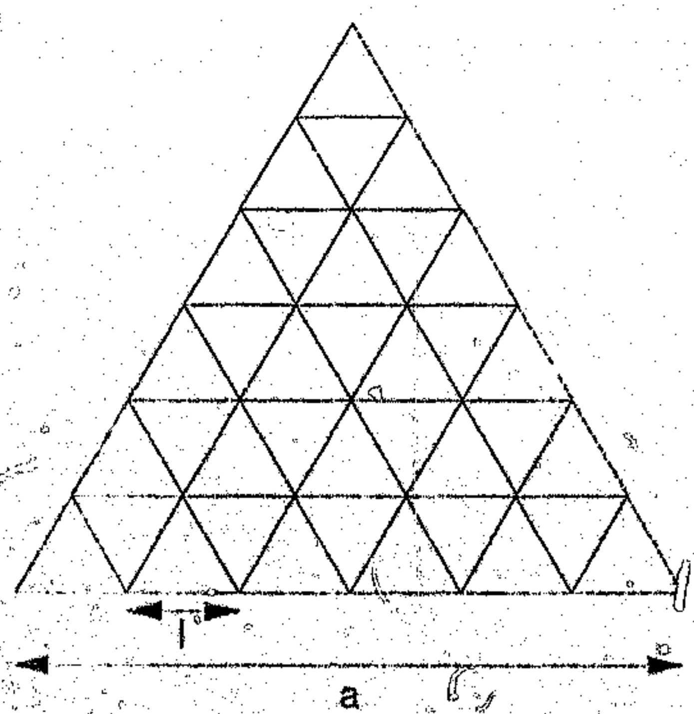

Figure E.1 Geometry of a triangular grid.

The surface of the triangular plate is $\frac{\sqrt{3}}{4}a^2$.

There are a total of $3\frac{a}{l}$ wires on the plate. The number of segments per wire varies from 1 to $\frac{a}{l}$. There are thus a total of $\frac{3}{2}\left(\frac{a}{l}+1\right)\frac{a}{l} \approx \frac{3}{2}\left(\frac{a}{l}\right)^2$ segments on the plate.

The area of a segment is $2\pi r l$.

As the total area of the wires must be equal to two times the area of the plate:

$$2\pi r l \cdot \frac{3}{2}\left(\frac{a}{l}\right)^2 = 2\frac{\sqrt{3}}{4}a^2$$

or

$$r = \frac{\sqrt{3}}{6\pi}l \approx 0.09l$$